

Kaon Condensation in a Nambu–Jona-Lasinio (NJL) Model at High Density

Michael McNeil Forbes

Center for Theoretical Physics, Department of Physics, MIT, Cambridge, Massachusetts 02139

(Dated: 30 November 2005)

We demonstrate a fully self-consistent microscopic realization of a kaon-condensed colour-flavour locked state (CFLK⁰) within the context of a mean-field NJL model at high density. The properties of this state are shown to be consistent with the QCD low-energy effective theory once the proper gauge neutrality conditions are satisfied, and a simple matching procedure is used to compute the pion decay constant, which agrees with the perturbative QCD result. The NJL model is used to compare the energies of the CFLK⁰ state to the parity even CFL state, and to determine locations of the metal/insulator transition to a phase with gapless fermionic excitations in the presence of a non-zero hypercharge chemical potential and a non-zero strange quark mass. The transition points are compared with results derived previously via effective theories and with partially self-consistent NJL calculations. We find that the qualitative physics does not change, but that the transitions are slightly lower.

I. INTRODUCTION

Recently there has been interest in the structure of matter at extremely high densities, such as might be found in the cores of neutron stars. At large enough densities, the nucleons are crushed together and the quarks become the relevant degrees of freedom. The asymptotic freedom of QCD ensures that the theory is weakly coupled at high enough densities. This allows one to perform weak-coupling calculations at asymptotically high densities. Such calculations have established that the structure of the ground state of quark matter is a colour superconductor (see for example [1, 2, 3, 4, 5, 6, 7, 8, 9, 10, 11, 12, 13, 14, 15]). In particular, at densities high enough that the three lightest quarks can be treated as massless, the ground state is the colour-flavour-locked (CFL) state in which all three colours and all three flavours participate in maximally (anti)-symmetric pairing [7, 10, 16, 17].

Determination of the QCD phase structure at moderate densities and in the presence of non-zero quark masses has proceeded in several ways. One approach has been to formulate a chain of effective theories, and then to match coefficients across several energy scales through these effective theories to perturbative calculations. Coefficients in the low-energy chiral effective theory [18] are matched to calculations performed in high-density effective theories (HDET) [9, 19, 20] which in turn are matched to weakly-coupled QCD. This allows one to determine the properties of the Goldstone bosons and determine the effects of small quark masses [21, 22, 23, 24, 25, 26, 27, 28, 29, 30]. Within this framework, it has been noted that, in the presence of a finite strange quark mass, neutral “kaons” (the lightest pseudo-Goldstone modes at high density with the same quantum numbers as their vacuum counterpart) can Bose-condense in the CFL state to form a kaon-condensed CFLK⁰ phase with lower condensation energy [31, 32, 33].

Unfortunately, the low-energy effective theory is only reliable for small perturbations and at moderate densities the strange quark mass is not a small perturbation.

A recent attempt has been made to extrapolate to large strange quark mass (m_s) [34], but this approach has not dealt with additional complications in the condensate structure that allow different gap parameters for each pair of quarks.

To deal with moderate quark masses, another approach has been to study Nambu–Jona-Lasinio (NJL) models [35, 36] of free quarks with contact interactions that model instanton interactions or single gluon exchange. These models are amenable to a mean-field treatment and exhibit a similar symmetry breaking pattern to QCD which results in CFL ground states [5, 6].

Within these models, one can study the effects of moderate quark masses through self-consistent solutions of the mean-field gap equations. This has led to a plethora of phases. In particular, several analyses show a transition to a colour-flavour locked phase with gapless fermionic excitations (the gCFL phase). These include both NJL-based calculations [37, 38, 39, 40] and effective-theory-based calculations [34, 41]. Until recently, however, the NJL calculations have excluded the possibility of kaon condensation (see however [42] which considers kaon condensation in the NJL model at low density), while the effective theories do not consider the complicated patterns in which the condensate parameters evolve at finite quark masses.

The goal of this paper is to show that one can combine the analysis of the low-energy effective theories, which exhibit kaon condensation, with the self-consistent mean-field analysis of the NJL model, which accounts for the full condensate structure. In particular, we use an NJL model based on single gluon exchange to find self-consistent solutions that correspond to the CFLK⁰ phase; we show that these phases agree with the predictions of the low-energy effective theory; and we determine how and where the zero temperature phase transition to a gapless CFL phase occurs as one increases the strange quark mass. In addition, unlike previous work on the NJL model, our numerical solutions are *fully* self-consistent: we include *all* condensates and self-energy corrections required to close the gap equations.

We first describe the pattern of symmetry breaking that leads to the CFL and CFLK⁰ states (Section II). Then we present our numerical results, demonstrating some properties of these states and determining the locations of the zero-temperature phase transitions (Section III). After a careful description of our model (Section IV) we derive the low-energy effective theory, paying particular attention to the differences between QCD and the NJL model (Section V). Here we demonstrate that, for small perturbations, our numerical solutions are well described by the effective theory, and we use our numerical results to compute the pion decay constant f_π which agrees with the perturbative QCD results. Specific numerical details about our calculations and a full description of our self-consistent parametrization are given in Appendix A.

We leave for future work the consideration of finite temperature effects, the analysis of the gapless CFLK⁰ (gCFLK⁰), the inclusion of instanton effects, the inclusion of up and down quark mass effects, and the possibility of other forms of meson condensation.

II. COLOUR FLAVOUR LOCKING (CFL)

QCD has a continuous symmetry group of $U(1)_B \otimes SU(3)_L \otimes SU(3)_R \otimes SU(3)_C$. In addition, there is an approximate $U(1)_A$ axial flavour symmetry that is explicitly broken by anomalies. At sufficiently high densities, however, the instanton density is suppressed and this symmetry is approximately restored.

The CFL ground state spontaneously breaks these continuous symmetries through the formation of a diquark condensate [7]

$$\langle \bar{\psi}_{\alpha a}^C \gamma_5 \psi_{\beta b} \rangle \propto \Delta_3 \epsilon^{\alpha\beta k} \epsilon_{abk} + \Delta_6 (\delta_a^\alpha \delta_b^\beta + \delta_b^\alpha \delta_a^\beta). \quad (1)$$

The symmetry breaking pattern (including the restored axial $U(1)_A$ symmetry) is thus¹

$$\frac{U(3)_L \otimes U(3)_R \otimes U(3)_C}{Z_3} \rightarrow SU(3)_{L+R+C} \otimes Z_2 \otimes Z_2 \quad (2)$$

where the Z_2 symmetries correspond to $\psi_L \rightarrow -\psi_L$ and $\psi_R \rightarrow -\psi_R$. It has been noted that the symmetry breaking pattern at high density (2) is the same as that for hyper-nuclear matter at low density [43]. This leads one to identify the low-energy pseudo-scalar degrees of freedom in both theories. We shall refer to the pseudo-scalar Goldstone bosons in the high-density phase as “pions” and “kaons” etc. when they have the same flavour quantum numbers as the corresponding low-density particles.

The CFL state (1) preserves parity, and is preferred when instanton effects are considered. Excluding instanton effects, there is an uncountable degeneracy of physically equivalent CFL ground states that violate parity. These are generated from the parity even CFL by the broken symmetry generators.

The symmetry breaking pattern (2) breaks 18 generators. The quarks, however, are coupled to the eight gluons associated with the $SU(3)_C$ colour symmetry and to the photon of the $U(1)_{EM}$ electromagnetism (which is a subgroup of the vector flavour symmetry). Eight of these gauge bosons acquire a mass through the Higgs mechanism and the coloured excitations are lifted from the low-energy spectrum. There remain 10 massless Nambu-Goldstone excitations: a pseudo-scalar axial flavour octet of mesons, a scalar superfluid boson associated with the broken $U(1)_B$ baryon number generator, and a pseudo-scalar η' boson associated with broken axial $U(1)_A$ generator. There remains one massless gauge boson that is a mixture of the original photon and one of the gluons [7, 44]. With respect to this “rotated electromagnetism” $U(1)_{\tilde{Q}}$ the CFL state remains neutral [45].

The degeneracy of the vacuum manifold is lifted by the inclusion of a non-zero strange quark mass m_s . In the absence of instanton effects and other quark masses, the ground state is not near to the parity even CFL state (1), but rather, is a kaon rotated state CFLK⁰. As $m_s \rightarrow 0$ this state approaches a state on the vacuum manifold that is a pure kaon rotation of the parity even CFL (1).

Even in the absence of quark masses, the vacuum manifold degeneracy is partially lifted by the anomalous breaking of the $U(1)_A$ axial symmetry which we have neglected: Instanton effects tend to disfavour kaon condensation by favouring parity even states, and thus delay the onset of the CFLK⁰ until m_s reaches a critical value (possibly excluding it). The effects of anomaly and instanton contributions have been well studied [6, 16, 26, 46, 47, 48] and play an important quantitative role in the phase structure of QCD. Non-zero up and down quark masses also tend to disfavour kaon condensation.

For the purposes of this paper, we shall neglect both the effects of instantons, and the effects of finite up and down quark masses. This will ensure that kaon condensation occurs for arbitrarily small m_s . Both of these effects open the possibility of a much richer phase structure, including condensation of other mesons (see for example [33, 49]). Future analyses should take these numerically important effects into account, both in the effective theory and in the NJL model.

The primary source of for kaon condensation is the finite strange quark mass. To lowest-order, this behaves as a chemical potential [31, 32, 33] (see (3) and (4)). In this paper, we also consider the addition of a hypercharge chemical potential as this removes many complications associated with masses and leads to a very clean demonstration of kaon condensation.

¹ The Z_3 factor mods out the common centres. See (10) for the explicit representation.

III. SELF-CONSISTENT SOLUTIONS

We consider four qualitatively different phases: Two are self-consistent mean-field solutions to the NJL model with a finite hypercharge chemical potential parameter μ_Y ; the other two are self-consistent mean-field solutions

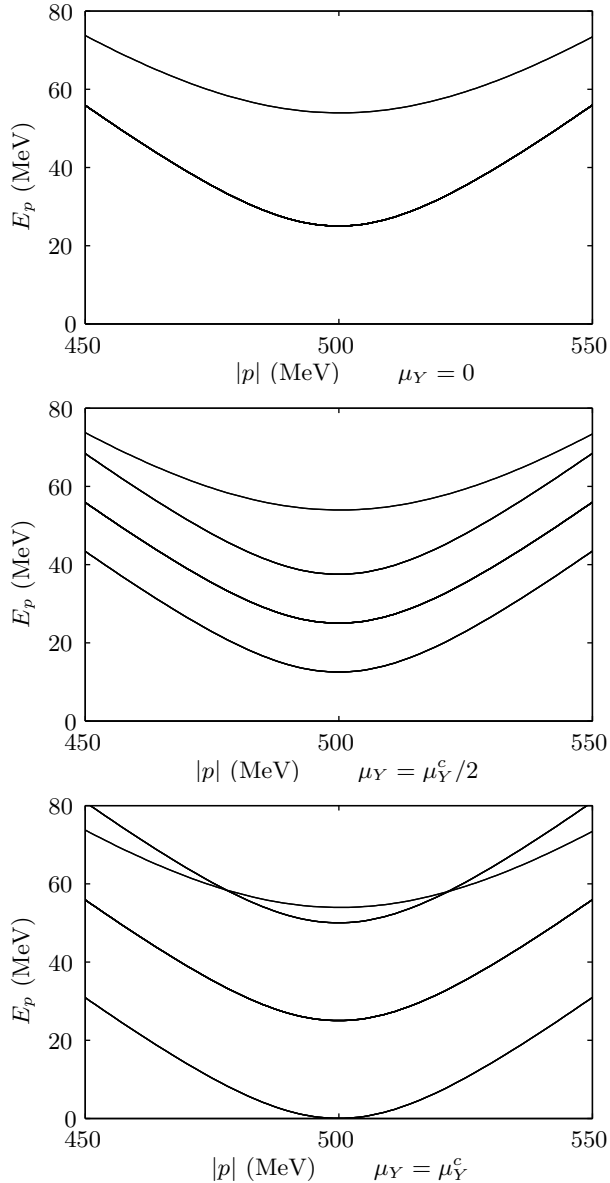


FIG. 1: Lowest lying quasiparticle dispersions about the Fermi momentum $p_F = \mu_q = 500$ MeV for the CFL phase with different values of the hypercharge chemical. All dispersions have left-right degeneracy: we now consider the colour-flavour degeneracy. In the top plot $\mu_Y = 0$, and the lowest dispersion has an eight-fold degeneracy and a gap of $\Delta_0 = 25$ MeV. The upper band contains a single quasiparticle pairing (ru,gd,bs) with a gap of $4\Delta_6 + 2\Delta_3 = 54$ MeV. In the middle plot, $\mu_Y = \mu_Y^c/2 = 12.5$ MeV, and (rs,bu) and (gs,bd) pairs are shifting as indicated in Table I. In the last plot, two pairs have become gapless marking the CFL/gCFL transition.

to the NJL model with a finite strange-quark mass parameter m_s . In each of these cases, one solution corresponds to a parity even CFL phase and the other corresponds to a kaon-condensed CFLK⁰ phase. Our normalizations and a complete description of the model are presented in Section IV. A full description of all the parameters required to describe these phases along with some typical values is presented in Appendix A.

	ru	gd	bs	rd	gu	rs	bu	gs	bd
CFL	0	0	0	0	0	-1	+1	-1	+1
CFLK ⁰	0	$+\frac{1}{2}$	$-\frac{1}{2}$	0	$+\frac{1}{2}$	-1	$+\frac{1}{2}$	$-\frac{1}{2}$	$+\frac{1}{2}$

TABLE I: Leading order shifts in the chemical potentials of the various quarks in the CFL and CFLK⁰ states in the presence of a hypercharge chemical potential shift μ_Y . This follows directly from (50).

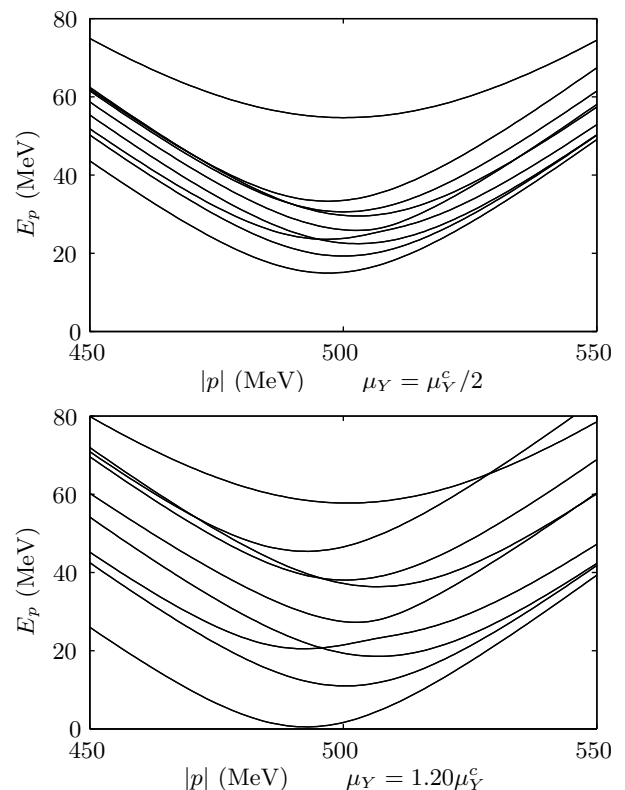


FIG. 2: Lowest lying quasiparticle dispersions about the Fermi momentum $p_F = \mu_q = 500$ MeV for the CFLK⁰ phase with different values of the hypercharge chemical. (The $\mu_Y = 0$ dispersions are the same as in the top of Figure 1.) Again, all dispersion have a left-right degeneracy. In the top plot at $\mu_Y = \mu_Y^c/2 = 12.5$ MeV, the eight-fold degenerate lowest band has split into eight independent dispersions. To leading order in the perturbation, the splitting is described by Table I, but the lack of degeneracy indicates that there are also higher order effects. The lower plot at $\mu_Y \approx 1.20\mu_Y^c \approx 30$ MeV is close to the CFLK⁰/gCFLK⁰ transition. The gapless band now contains only a single mode and is charged.

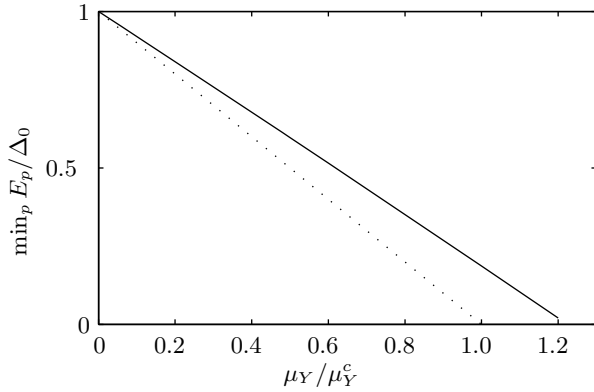


FIG. 3: Physical gap of the lowest lying excitation as a function of the hypercharge chemical potential. The dotted line corresponds to the CFL phase: the phase transition to the gCFL occurs at $\mu_Y = \mu_Y^c$ where the gap vanishes. The solid line corresponds to the CFLK⁰ state. The transition to a gapless phase is delayed by a factor of 1.22.

A. Finite Hypercharge Chemical Potential

The CFL phase in the presence of a hypercharge chemical potential corresponds to the fully gapped CFL phase discussed in [37]. Here one models the effects of the strange quark through its shift on the Fermi surface $p_F \approx \mu_q$ of the strange quarks. This can be seen by expanding the free-quark dispersion

$$\sqrt{p^2 + M_s^2} \approx |p| + \frac{M_s^2}{2\mu_q} + \dots \quad (3)$$

or, more carefully, by integrating out the antiparticles to formulate the High-Density Effective Theory. (See for example [9, 19, 20, 30].) These leading order effects are equivalent to adding a hypercharge chemical potential of magnitude

$$\mu_Y = \frac{M_s^2}{2\mu_q}. \quad (4)$$

and a baryon chemical potential shift of

$$\delta\mu_B = -\frac{M_s^2}{\mu_q}. \quad (5)$$

We consider only the effect of the hypercharge chemical potential here, holding μ_B fixed. Note that the relevant parameters are M_s and μ_q rather than m_s and $\mu_s = \mu_B/3$. M_s is the constituent quark mass that appears in the dispersion relation whereas m_s is the bare quark mass parameter; likewise, μ_q is the corrected quark chemical potential that determines the Fermi surface whereas $\mu_s = \mu_B/3$ is the bare baryon chemical potential. (These distinctions are important because our model takes into account self-energy corrections.)

The CFL phase responds in a trivial manner to a hypercharge chemical potential: the quasiparticle dis-

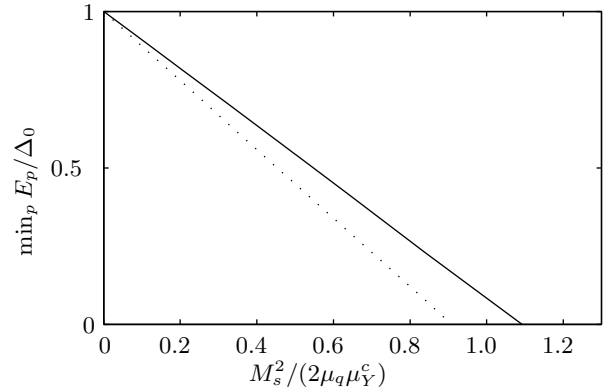


FIG. 4: Physical gap of the lowest lying excitation as a function of the strange quark mass. The dotted line corresponds to the CFL phase and the solid line corresponds to the CFLK⁰ phase. We have normalized the axes in terms of $\mu_Y^c = \Delta_0$ for comparison with the hypercharge chemical potential case. The CFL/gCFL transition occurs at a slightly smaller value of $M_s^2/\mu_q \approx 45.4$ MeV than the value of 46.8 MeV in [37, 38, 40]. This is due to the effects of the other parameters on the quasiparticle dispersion relations. We note that, as with μ_Y , the transition from the CFLK⁰ to a gapless phase is delayed relative to the CFL/gCFL transition, but by a slightly reduced factor of 1.2. This is in qualitative agreement but quantitative disagreement with the factor of 4/3 found in [34]. The is most-likely the result of our fully self-consistent treatment of the condensate parameters.

persions shift such that the physical gap in the spectrum becomes smaller; none of the other physical properties change. In particular, as the hypercharge chemical potential increases, the coloured chemical potential $\mu_8 = -\mu_Y$ decreases to maintain neutrality. The values of all of the gap parameters, the self-energy corrections, the densities and the thermodynamic potential remain unchanged until the physical gap in the spectrum vanishes. (The apparent change in the magnitude of the gap parameters in the first figure of [37] is due to the shift in the baryon chemical (5) which occurs if one uses the strange quark chemical potential shift μ_s rather than a hypercharge shift μ_Y .) This is a consequence of the \tilde{Q} neutrality of the CFL state [50]. In particular, the electric chemical potential remains zero $\mu_e = 0$ and the state remains an insulator until the onset of the gapless modes. The same phenomena has also been noticed in the two-flavour case [51, 52, 53]. As such, we can analytically identify the phase transition to the gCFL phase which occurs for the critical chemical potential

$$\mu_Y^c = \Delta_0 \quad (6)$$

where $\Delta_0 = \Delta_3 - \Delta_6$ is the physical gap in the spectrum in the absence of any perturbations. Throughout this paper we use parameters arbitrarily chosen so that $\mu_Y^c = \Delta_0 = 25$ MeV to correspond with the parameter values in [37, 38, 40]. We show typical quasiparticle dispersion relations for this state in Figure 1.

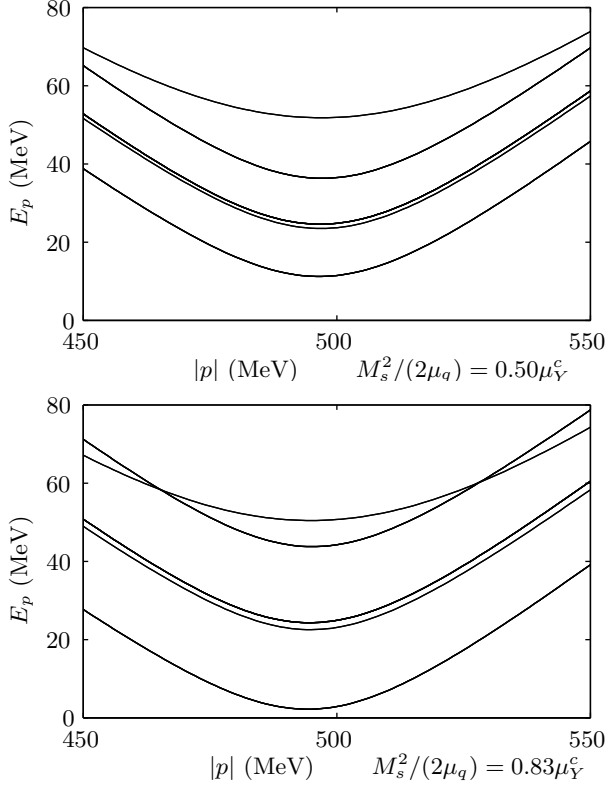


FIG. 5: Lowest lying quasiparticle dispersion relationships about the Fermi momentum $p_F = \mu_q = 500$ MeV for the CFL phase with two different values of the strange quark mass. (The $M_s = 0$ dispersions are the same as in the top of Figure 1.) Qualitatively this has the same structure as Figure 1 except that middle dispersion is now split by higher order mass effects.

The splitting of the dispersions can also be easily understood from the charge neutrality condition (50) and the leading order effects are summarized in Table I. After setting $\mu_8 = -\mu_Y$, the chemical potentials for the rs and gs quarks shift by $-\mu_Y$ whereas for the bu and bd quarks it shifts by $+\mu_Y$. Thus, the (gs,bd) and (rs,bu) pairs are the first to become gapless.

The kaon-condensed hypercharge state is more complicated. One can again use the appropriate charge neutrality conditions (50) to estimate how the quarks will be affected by μ_Y , but the naïve results hold only to lowest-order. In particular, the condensates of the CFLK⁰ state also vary as μ_Y increases (see Table III). These higher order effects break all the degeneracy between the quark species and Figure 2 has nine independent dispersions.

We shall compare the thermodynamic potentials of these two states later (see Figures 7 and 8), but we point out here that the transition to a gapless colour-flavour-locked state with kaon condensation (gCFLK⁰) occurs at a larger hypercharge chemical potential than the CFL/gCFL transition. This can be most easily seen in Figure 3. This is in qualitative agreement with [34] and [41], but in quantitative disagreement.

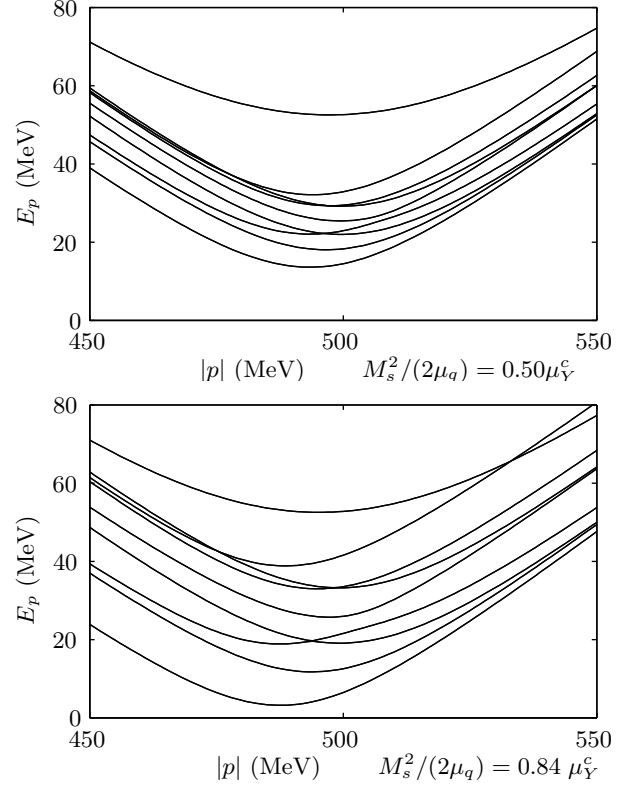


FIG. 6: Lowest lying quasiparticle dispersion relationships about the Fermi momentum $p_F = \mu_q = 500$ MeV for the CFLK⁰ phase with two different values of the strange quark mass. (The $M_s = 0$ dispersions are the same as in the top of Figure 1.) Qualitatively this has the same structure as Figure 2.

In the CFL/gCFL transition, two modes become gapless simultaneously: the lower branches of the (rs,bu) and (gs,bd) pairs. One of these modes is electrically neutral (gs,bd) and it crosses the zero-energy axis giving rise to a “breach” in the spectrum. The other mode is electrically charged: as soon as it crosses, the electric chemical potential must rise to enforce neutrality. The state now contains gapless charged excitations and becomes a conductor. The result is that the neutral gapless mode has two linear dispersions while the charged gapless mode has a virtually quadratic dispersion when electric neutrality is enforced. (This was discovered in [37] and is explained in detail in [38].)

In the CFLK⁰/gCFLK⁰ transition, a single charged mode becomes gapless.² Thus, immediately beyond the

² This mode pairs rs, gu, and bu quarks in quite a non-trivial manner. In the CFL, the quasiparticles form a nice block-diagonal structure in which the quarks exhibit definite pairing between two species. In the CFLK⁰, the block structure is more complicated and the pairing cannot be simply described: the lowest lying quasiparticle is a linear combination of the three rs, gu, and bu quark.

transition, the corresponding gCFLK⁰ state will also be a conductor but there will be a single charged gapless mode with almost quadratic dispersion. Additional modes will continue to lower until either more modes become gapless, or a first order phase transition to a competing phase occurs.

B. Finite Strange Quark Mass

The second pair of CFL/CFLK⁰ states that we consider are self-consistent solutions to the gap equation in the presence of a finite strange quark mass. Qualitatively we expect to see similar features to the states at finite hypercharge chemical potential and indeed we do as shown in Figures 5 and 6.

Quantitatively, we notice a few differences with previous analyses concerning the locations of the phase transitions to gapless states. Our parameters have been chosen to match the parameters in [37, 38, 40]. They find that the gCFL/CFL transition occurs at $M_s^2/\mu = 46.8$ MeV, but the CFL/gCFL transition happens noticeably earlier with our model at $M_s^2/\mu = 43.9$ MeV. This is due to a corresponding six-percent reduction in the condensate parameters and represents the effects of performing a fully self-consistent calculation.

Another difference concerns the appearance of gapless modes in the CFLK⁰ state (see Fig. 4). This transition occurs at $M_s^2/\mu = 52.5$ MeV in our model—a factor of 1.2 larger than the CFL/gCFL transition. This is some ten percent smaller than the factor of 4/3 derived in [34]. This is likely due to the more complicated condensate structure we consider and the inclusion of self-energy corrections.

IV. NJL MODEL

We base our analysis on the following Hamiltonian for the NJL model

$$H = \int \frac{d^3\vec{p}}{(2\pi)^3} \psi_{\vec{p}}^\dagger (\vec{\alpha} \cdot \vec{p} - \mu + \gamma_0 \mathbf{M}) \psi_{\vec{p}} + H_{\text{int}}. \quad (7)$$

Here we consider 9 species of quarks = 3 colours \times 3 flavours: Including the relativistic structure, there are 36 quark operators in the vector ψ . The matrices μ and \mathbf{M} are the quark chemical potentials and masses respectively.

We take the interaction to be a four-fermion contact interaction with the quantum numbers of single gluon exchange:³

$$H_{\text{int}} = g \int (\bar{\psi} \gamma^\mu \lambda^A \psi) (\bar{\psi} \gamma_\mu \lambda^A \psi). \quad (8)$$

³ Here the matrices λ^A are the eight 3×3 Gell-Mann matrices and the γ^μ are the Dirac matrices which we take in the chiral basis.

The Gell-Mann matrices act on the colour space and the flavour structure is diagonal. We point out that this form of NJL interaction has the desirable feature of explicitly breaking the independent colour $SU(3)_{\text{CL}}$ left and $SU(3)_{\text{CR}}$ right symmetries that some NJL models preserve. This is important because the condensation pattern (1) does not explicitly link left and right particles: Our model thus has the same continuous symmetries as QCD, and the only complication to deal with is the gauging of the single colour $SU(3)_C$ symmetry.

Our goal here is to provide a non-perturbative model to discuss the qualitative features of QCD at finite densities. We model the finite density by working in the grand thermodynamic ensemble and introducing a baryon chemical potential for all of the quarks:

$$\mu = \frac{\mu_B}{3} \mathbf{1}. \quad (9)$$

With only this chemical potential and no quark masses, our model has an $U(3)_L \otimes U(3)_R \otimes SU(3)_C / Z_3$ continuous global symmetry in which the left-handed quarks transform as $(\bar{\mathbf{3}}, \mathbf{1}, \mathbf{3})$ and the right handed quarks transform as $(\mathbf{1}, \bar{\mathbf{3}}, \mathbf{3})$. In the chiral basis we have explicitly⁴

$$\begin{pmatrix} \psi_L \\ \psi_R \end{pmatrix} \rightarrow \begin{pmatrix} e^{-i\theta_L} \mathbf{F}_L^* \otimes \mathbf{C} & \mathbf{0} \\ \mathbf{0} & e^{-i\theta_R} \mathbf{F}_R^* \otimes \mathbf{C} \end{pmatrix} \begin{pmatrix} \psi_L \\ \psi_R \end{pmatrix} \quad (10)$$

where \mathbf{F} and \mathbf{C} are $SU(3)$ matrices. For an attractive interaction, this NJL model exhibits the same symmetry breaking pattern as QCD (2) with a restored axial symmetry. The difference between this NJL model and QCD is that the NJL model contains no gauge bosons. Thus, there are 18 broken generators which correspond to massless Goldstone bosons, and none of these is eaten. To effectively model QCD, we must remove the extra coloured Goldstone bosons. At the mean-field level, this is done by imposing gauge neutrality conditions [45, 54, 55]. Once the appropriate chemical potentials are introduced, the dependence on the vacuum expectation values of the coloured Goldstone modes is cancelled and the low-energy physics of the NJL model matches that of QCD.

The usual NJL model has a local interaction, but this is not renormalizable and needs regulation. For the purposes of this paper, we introduce a hard cutoff on each

Our normalizations and conventions are

$$\begin{aligned} \text{Tr}[\lambda^A \lambda^B] &= \frac{1}{2} \delta^{AB}, \\ \gamma_5 &= i\gamma_0 \gamma_1 \gamma_2 \gamma_3 = \begin{pmatrix} -1 & \mathbf{0} \\ \mathbf{0} & 1 \end{pmatrix}, \\ \gamma_C &= i\gamma_2 \gamma_0. \end{aligned}$$

We also use natural units where $c = \hbar = k_B = 1$.

⁴ From this explicit representation we can see how the centres of the colour and flavours overlap giving rise to the Z_3 factor.

of the momenta $\Lambda_{\vec{p}} = \theta(\Lambda - \|\vec{p}\|)$ to mimic the effects of asymptotic freedom at large momenta:

$$H_{\text{int}} = \frac{g}{(2\pi)^9} \int d^3\vec{p} d^3\vec{p}' d^3\vec{q} d^3\vec{q}' \Lambda_p \Lambda_{p'} \Lambda_q \Lambda_{q'} \times \\ \times \delta^{(3)}(\vec{p} - \vec{p}' + \vec{q} - \vec{q}') (\bar{\psi}_{\vec{p}} \gamma^\mu \lambda^A \psi_{\vec{p}'})(\bar{\psi}_{\vec{q}} \gamma_\mu \lambda^A \psi_{\vec{q}'}).$$

To study this model we perform a variational calculation by introducing the quadratic Hamiltonian

$$H_0 = \int \frac{d^3\vec{p}}{(2\pi)^3} \left(\psi_{\vec{p}}^\dagger \mathbf{E}(\vec{p}) \psi_{\vec{p}} + \psi_{\vec{p}}^T \mathbf{B} \psi_{\vec{p}} + \psi_{\vec{p}}^\dagger \mathbf{B}^\dagger \psi_{\vec{p}}^* \right) \quad (11)$$

where

$$\mathbf{E}(\vec{p}) = \vec{\alpha} \cdot \vec{p} - \mu + \gamma_0 \mathbf{M} - \mathbf{A} \quad (12)$$

and then computing the following upper bound [56] on the thermodynamic potential Ω of the full system:

$$\Omega \leq \Omega_0 + \langle H - H_0 \rangle_0. \quad (13)$$

Ω_0 is the thermodynamic potential of the quadratic model and the expectation value $\langle \rangle_0$ is the thermal average with respect to the quadratic ensemble defined by H_0 . In principle, the quadratic model is exactly solvable, thus the upper bound can be computed. One then varies the parameters \mathbf{A} and \mathbf{B} to minimize this upper bound, obtaining a variational approximation for the true ensemble. In the zero-temperature limit, this is equivalent to simply minimizing the expectation value of the Hamiltonian over the set of all Gaussian states.

In practice, it is difficult to vary with respect to all possible quadratic models since the space is of uncountable dimensionality. In this paper we restrict ourselves to minimizing over homogeneous and isotropic systems. This is equivalent to performing a fully self-consistent mean-field analysis. The condition for the right hand side of (13) to be stationary with respect to the variational parameters is equivalent to the self-consistent gap equation.

The microscopic analysis presented in this paper consists of choosing reasonable parameterizations of \mathbf{A} (which includes the chemical potentials, masses and related corrections) and \mathbf{B} (which includes the gap parameters Δ) that are closed under the self-consistency condition, and numerically finding stationary points of this system of equations. (As \mathbf{A} and \mathbf{B} are arbitrary 36×36 matrices subject only to $\mathbf{A} = \mathbf{A}^\dagger$ and $\mathbf{B} = -\mathbf{B}^T$, a full parametrization consists of 2556 parameters and was too costly for the present author to consider. However, the parametrization chosen is quite natural and *fully* closed.) Once the parameters \mathbf{A} and \mathbf{B} are found, the properties of the ensemble can be computed by diagonalizing the quadratic Hamiltonian.

As discussed in Section V E and [45], we must impose the appropriate gauge charge neutrality conditions. This is done by introducing bare gauge chemical potentials into the model and choosing these to ensure the final solution is neutral.

To impose a charge neutrality condition, we instead vary μ_R (along with the other parameters) to obtain a neutral solution (again we note that the total charge and other correlations of the state depend only on the corrected parameters μ_R). Once this solution is found, $\delta\mu$ is computed and the required bare chemical potential $\mu = \mu_R - \delta\mu$ determined. Despite the fact that the self-energy corrections depend only on the corrected parameters (μ_R etc.), the thermodynamic potential depends on both the corrected and the bare parameters and so this last step is important.

One must also be careful about which thermodynamic potential is used to compare states when neutrality conditions are enforced as we are no longer in the grand ensemble. The differences between the potentials of the relevant ensembles are proportional to terms of the form $Q\mu$, however, so for neutrality conditions, $Q = 0$, and the thermodynamic potential may still be used to compare states.

A. Numerical Techniques

We sketch here the method used to calculate the thermodynamic potential and perform the variational minimization. First, we express the Hamiltonian H in the following simplified form

$$H = \Psi^\dagger \mathbf{H} \Psi + g \Psi^\dagger \mathbf{\Gamma}^\dagger \Psi \Psi^\dagger \mathbf{\Gamma} \Psi \quad (14)$$

where \mathbf{H} is a hermitian matrix. In order to do this and include the “anomalous” correlations $\langle \psi \psi \rangle$, we must use an augmented “Nambu-Gorkov” spinor

$$\Psi = \begin{pmatrix} \psi \\ \psi^C \end{pmatrix}, \quad (15)$$

where ψ^C is the charge conjugated spinor. This doubling of the degrees of freedom requires careful attention to avoid double counting.

To simplify the presentation of our method in this section, we shall ignore this complication and assume that Ψ contains a single set of operators with no duplicate degrees of freedom. We also consider only a single interaction term, and subsume the momentum structure into the matrix structure. Explicitly dealing with these complications is straightforward and the details are presented in [57].⁵

⁵ To derive the full equations, one introduces the augmented structure while imposing constraints on the matrices throughout the variation. For example, one must ensure that $\mathbf{H} = -\mathbf{C}\mathbf{H}^T\mathbf{C}$ where $\Psi^C = \mathbf{C}\Psi$. To derive the proper momentum structure, one simply attaches momentum indices: for homogeneous states all correlations have the form $\langle \Psi_{\vec{p}}^\dagger \Psi_{\vec{q}} \rangle \propto \delta^3(\vec{p} - \vec{q})$ and the momentum structure follows trivially.

We now express the variational Hamiltonian as

$$H_0 = \Psi^\dagger (\mathbf{H} + \mathbf{\Sigma}) \Psi = \Psi^\dagger \mathbf{H}_0 \Psi. \quad (16)$$

The matrix of variational parameters $\mathbf{\Sigma}$ may be thought of as the self-energy corrections. All of the two-point correlations are determined from the corrected Hamiltonian matrix \mathbf{H}_0 , with the “anomalous” correlations being found off the diagonal:

$$\langle \Psi \Psi^\dagger \rangle = \mathbf{F}^-, \quad \langle \Psi^* \Psi^T \rangle = [\mathbf{F}^+]^T, \quad \mathbf{F}^\pm = \frac{1}{1 + e^{\pm \beta \mathbf{H}_0}}.$$

At finite temperatures, there is a one-to-one relationship between \mathbf{E} and the matrix $\mathbf{F}^- = \mathbf{1} - \mathbf{F}^+$. Armed with this result, the variational bound takes the explicit form⁶

$$\Omega \leq \frac{1}{\beta} \text{Tr} \ln[\mathbf{F}^-] - \text{Tr}[\mathbf{\Sigma} \mathbf{F}^+] + g \left(\text{Tr}[\mathbf{\Gamma}^\dagger \mathbf{F}^+] \text{Tr}[\mathbf{\Gamma} \mathbf{F}^+] + \text{Tr}[\mathbf{\Gamma}^\dagger \mathbf{F}^- \mathbf{\Gamma} \mathbf{F}^+] \right). \quad (17)$$

From this, one may find the stationary points by differentiating with respect to \mathbf{F}^+ . At finite temperature this is formally equivalent to finding the stationary points by varying with respect to $\mathbf{\Sigma}$. Differentiating with respect to $\mathbf{\Sigma}$ is complicated by the functional dependence and the result is not expressible as a simple matrix equation. The conditions $\partial \Omega / \partial F_{ij}^+ = 0$ yield the fully self-consistent Schwinger-Dyson equations which may be expressed as:

$$\mathbf{\Sigma} = g \left(\mathbf{\Gamma}^\dagger \text{Tr}[\mathbf{\Gamma} \mathbf{F}^+] + \mathbf{\Gamma} \text{Tr}[\mathbf{\Gamma}^\dagger \mathbf{F}^+] + \mathbf{\Gamma}^\dagger \mathbf{F}^- \mathbf{\Gamma} - \mathbf{\Gamma} \mathbf{F}^+ \mathbf{\Gamma}^\dagger \right). \quad (18)$$

In principle, one may derive analytic expressions for these equations, but, in practise, the matrices are 72×72 and computing \mathbf{F}^\pm analytically—even when many approximations are made—is quite tedious. Instead, we simply use these expressions numerically. The required diagonalization is then efficiently performed using standard numerical linear algebra tools. The traces involved include momentum integrals, but for homogeneous states these are one-dimensional and thus also quite efficient. The biggest challenge is to solve simultaneously the equations present in (18). This is done by first projecting out the limited subspaces describe in Appendix A and then employing a multi-dimensional root-finder.

Since the search space is large (~ 45 parameters for the CFLK⁰ states), traditional root-finders are prohibitive because they recompute the Jacobian at each step. Here we use a modified Broyden algorithm [58, 59] to provide

a secant-like update to the Jacobian requiring far fewer function evaluations per step of the algorithm.

In many cases, the Schwinger-Dyson equation (18) converges through simple iteration. With charge neutrality constraints, this is often no longer the case, but the Broyden update is sufficient to restore convergence.

B. CFL at $m_s = 0$.

As an example, consider the parity even CFL state. The self-consistency conditions are fully closed when one includes four variational parameters. There are two gap parameters Δ_3 and Δ_6 corresponding to the diquark condensate (1), one chemical potential correction $\delta\mu_B$ to the baryon chemical potential and an induced off-diagonal chemical potential μ_{oct} . The quadratic Hamiltonian (11) can thus be expressed

$$H_0 = \psi^\dagger \left(\vec{\alpha} \cdot \vec{p} - \frac{1}{3} \mu_B - \delta\mu \right) + \frac{1}{2} \psi^T \gamma_C \gamma_5 \Delta \psi + \text{h.c.}$$

where

$$[\Delta]^{aa}_{bb} = \Delta_3 \epsilon^{\alpha\beta k} \epsilon_{abk} + \Delta_6 (\delta_a^\alpha \delta_b^\beta + \delta_b^\alpha \delta_a^\beta), \quad (19)$$

$$\delta\mu = \frac{1}{3} \delta\mu_B + \mu_{\text{oct}}, \quad (20)$$

and

$$[\mu_{\text{oct}}]^{aa}_{bb} = \mu_{\text{oct}} \left(\sum_{A=1}^8 [\lambda^A]_{\alpha a} [\lambda^A]_{\beta b} - 8 [\lambda^0]_{\alpha a} [\lambda^0]_{\beta b} \right).$$

Most of this structure is all well-known and discussed many times in the literature, however, there has been no mention of the parameter μ_{oct} because most analyses neglect the self-energy corrections.

Neglecting the correction to the baryon chemical potential is reasonable since it has little physical significance: it simply enters as a Lagrange multiplier to establish a finite density. As such, the effective common quark chemical potential

$$\mu_q = \frac{1}{3} \mu_B^{\text{eff}} = \frac{1}{3} (\mu_B + \delta\mu_B) \quad (21)$$

is the relevant physical parameter defining the Fermi surface. To compare states in the grand ensemble, however, one must fix the bare rather than the effective chemical potentials. This is what we have done in our calculations. Numerically, we find that the corrections $\delta\mu_B$ cause μ_q to vary by only a few percent as we vary the perturbation parameters μ_Y and m_s .

There is no bare parameter corresponding to μ_{oct} . Thus, it is spontaneously induced and should be treated on the same footing as Δ . To see that such a parameter must exist, consider changing to the “octet” basis using the augmented Gell-Mann matrices

$$\tilde{\psi}_A = 2[\lambda^A]_{\alpha a} \psi_{(\alpha a)} \quad (22)$$

⁶ For a fully self-consistent analysis, we must include the term $-g \langle \Psi^\dagger \Psi^\dagger \rangle \langle \Psi \Psi \rangle$. These correlations vanish in this simplified analysis, but are included when the full augmented structure (15) is considered as discussed in [57]. Note also that momentum integration is implicit in the matrix multiplication and traces.

where $\lambda^0 = 1/\sqrt{6}$. In this basis, the off-diagonal condensate becomes diagonal with one singlet parameter $4\Delta_6 + 2\Delta_3$ and eight octet parameters $\Delta_6 - \Delta_3$:

$$\tilde{\Delta} = \begin{pmatrix} 4\Delta_6 + 2\Delta_3 & & & \\ & \Delta_6 - \Delta_3 & & \\ & & \ddots & \\ & & & \Delta_6 - \Delta_3 \end{pmatrix} \quad (23)$$

It is clear that in the CFL, the singlet channel decouples from the octet channel: there is no symmetry relating these and the two gap parameters are related by the numerical value of the coupling g . This decoupling is also present in the chemical potential corrections. One linear combination corresponds to the identity: this corrects the baryon chemical potential $\delta\mu_B$. The other is the induced μ_{oct} .

Numerically, we calibrate our model with this CFL solution. In particular, we chose our parameters to reproduce the results of [40]. We use a hard cutoff at $\Lambda = 800$ MeV, and a coupling constant chosen so that, with an effective quark chemical potential of $\mu_q = 500$ MeV one has a physical gap in the spectrum of $\Delta_0 = \Delta_3 - \Delta_6 = 25$ MeV. This fixes the following parameter values which we hold fixed for all of our calculations:

$$\Lambda = 800 \text{ MeV}, \quad (24a)$$

$$g\Lambda^2 = 1.385, \quad (24b)$$

$$\mu_B/3 = 549.93 \text{ MeV}. \quad (24c)$$

With these parameters fixed, the fully self-consistent mean-field CFL solution has the following variational parameters:

$$\Delta_3 = 25.6571 \text{ MeV},$$

$$\Delta_6 = 0.6571 \text{ MeV},$$

$$\delta\mu_B/3 = -49.93 \text{ MeV},$$

$$\mu_{\text{oct}} = -0.03133 \text{ MeV}.$$

As first noted in [7], and discussed in [60], the parameter Δ_6 is required to close the gap equation, but is small because the sextet channel is repulsive. In weakly-coupled QCD, Δ_6 is suppressed by an extra factor of the coupling. This effect is numerically captured in the NJL model. The parameter μ_{oct} is also required to close the gap equation when the Hartree-Fock terms are included. It is also numerically suppressed. Recent calculations often omit Δ_6 and μ_{oct} : we see that this is numerically justified.

The physical gap in the spectrum also defines the critical hypercharge chemical potential for the CFL/gCFL transition (6):

$$\mu_Y^c = \Delta_0 = 25.00 \text{ MeV}. \quad (26)$$

C. CFL at $\mu_Y, m_s \neq 0$

Once one introduces a strange quark mass, one must introduce additional parameters. A simple way to determine which parameters are required is to add the mass, then compute the gap equation and see which entries in the self-energy matrix are non-zero. By doing this for a variety of random values of the parameters, one can determine the dimension of the subspace required to close the gap equation and introduce the required parameters.

In the case of the CFL state with non-zero hypercharge chemical potential, one only needs to introduce the parameters μ_Y and μ_8 to ensure gauge neutrality: As discussed in Sec. III A, none of the other parameters change. To go beyond the transition into the gCFL phase, however, or to extend the results to non-zero temperature, one must introduce additional parameters. These include the perturbation μ_Y , the gauge chemical potentials μ_3 , μ_8 , and μ_e required to enforce neutrality, as well as nine gap parameters Δ_{12} , Δ_{23} , Δ_{13} , Δ_{45} , Δ_{67} , Δ_{89} , Δ_{11} , Δ_{22} , and Δ_{33} that fully parametrize the triplet and sextet diquark condensates. (These latter nine parameters correspond to the parameters ϕ_i , φ_i and σ_i defined in reference [39].) The additional parameters are chemical potentials similar to μ_{oct} which are induced by the gap equations. The full set of parameters is discussed in Appendix A.

Adding a strange quark mass is more complicated. First of all, we need to introduce additional Lorentz structure. For homogeneous and isotropic systems, there are eight possible relativistic structures:

$$\mathbf{A} = \mathbf{1} \otimes \delta\mu + \gamma_5 \otimes \delta\mu_5 - \gamma_0 \otimes \delta\mathbf{m} - \gamma_0\gamma_5 \otimes \delta\mathbf{m}_5,$$

$$\mathbf{B} = \gamma_C\gamma_5 \otimes \Delta + \gamma_C \otimes \Delta_5 + \gamma_0\gamma_C\gamma_5 \otimes \kappa + \gamma_0\gamma_C \otimes \kappa_5.$$

Introducing quark masses requires one to introduce the additional Lorentz structure κ [60] to close the gap equations, but these are found to be small. In total, one requires about 20 parameters to fully parametrize the CFL in the presence of a strange quark mass (see Table IV).

With the inclusion of a bare quark mass m_s one induces a chiral condensate $\langle\bar{\psi}\psi\rangle$ which in turn generates a correction to the quark mass. The resulting parameter in \mathbf{H}_0 (11) is the constituent quark mass M_s which appears in the dispersion relationships for the quarks. It is this constituent quark mass that must be used when calculating the effective chemical potential shift (4). Generally the constituent quark mass is quite a bit larger than the bare quark mass parameter m_s . For example, close to the phase transition, we have $m_s \approx 83$ MeV while the constituent quark mass is $M_s \approx 150$ MeV (see Table IV). We have checked that our calculations are quantitatively consistent with the calculations presented in [61] in this regard.

D. CFLK⁰

Applying a kaon rotation to the CFL state breaks the parity of the state, and mixes the parity even parameters μ , \mathbf{m} , Δ and κ with their parity odd counterparts μ_5 , \mathbf{m}_5 , Δ_5 and κ_5 . The full set of parameters and typical numerical values is presented in Appendix A.

V. LOW-ENERGY EFFECTIVE THEORY

To describe the low-energy physics of these models, we follow a well established procedure: identify the low-energy degrees of freedom and their transformation properties, identify the expansion parameters (power counting scheme), write down the most general action consistent with the symmetries and power counting, and determine the arbitrary coefficients by matching to experiment or another theory. In our case, we will match onto the mean-field approximation of the NJL model. The resulting low-energy effective theory has been well studied [18, 62]: we use this presentation to establish our conventions, and to contrast the effective theory of QCD with that of the microscopic NJL model.

A. Degrees of Freedom

The coset space in the NJL model is isomorphic to $U(3) \otimes U(3)$. This can be fully parametrized with two $SU(3)$ matrices \mathbf{X} and \mathbf{Y} and two physical phases A and V which one can physically identify with the condensates:

$$\sqrt{V^\dagger A} [\mathbf{X}]_{c\gamma} \propto \epsilon_{abc} \epsilon_{\alpha\beta\gamma} \langle \psi_L^{a\alpha} \psi_L^{b\beta} \rangle, \quad (27a)$$

$$\sqrt{V^\dagger A^\dagger} [\mathbf{Y}]_{c\gamma} \propto \epsilon_{abc} \epsilon_{\alpha\beta\gamma} \langle \psi_R^{a\alpha} \psi_R^{b\beta} \rangle. \quad (27b)$$

These thus transform as follows:

$$\mathbf{X} \rightarrow \mathbf{F}_L \mathbf{X} \mathbf{C}^\dagger, \quad (28a)$$

$$\mathbf{Y} \rightarrow \mathbf{F}_R \mathbf{Y} \mathbf{C}^\dagger, \quad (28b)$$

$$A \rightarrow e^{2i(\theta_R - \theta_L)} A, \quad (28c)$$

$$V \rightarrow e^{2i(\theta_R + \theta_L)} V. \quad (28d)$$

Note that the condensation pattern $\mathbf{X} = \mathbf{Y} = \mathbf{1}$, $A = V = 1$ is unbroken by the residual symmetry where $\mathbf{F}_L = \mathbf{F}_R = \mathbf{C}$ and also by the Z_2 symmetries where $\theta_L, \theta_R = \pm\pi$. This is the reason for the extra factor of two in the phases. In QCD the degrees of freedom are similar, but one must consider only colour singlet objects. Thus, the low-energy theory for QCD should include only the colour singlet combination

$$\Sigma = \mathbf{X} \mathbf{Y}^\dagger \rightarrow \mathbf{F}_L \Sigma \mathbf{F}_R^\dagger \quad (29)$$

and the colour singlet phases A and V . Note also that these have the following transformation properties under

parity

$$\mathbf{X} \leftrightarrow \mathbf{Y}, \quad \mathbf{A} \leftrightarrow \mathbf{A}^\dagger, \quad \Sigma \leftrightarrow \Sigma^\dagger. \quad (30a)$$

The field content of the effective theories is thus:

H, η' : Two singlet fields corresponding to the $U(1)$ phases of A and V . The field associated with V is a scalar boson associated with the superfluid baryon number condensation. We shall denote this field H .

The field associated with A is a pseudo-scalar boson associated with the axial baryon number symmetry and shall be identified with the η' particle. As discussed in Section II, the axial symmetry symmetry is anomalously broken in QCD and the η' is not strictly massless due to instanton effects, but these are suppressed at high density. We ignore these effects. Our NJL model thus contains no instanton vertex and our low-energy theory will contain no Wess-Zumino-Witten terms [63, 64]. It would be interesting to include both of these terms and repeat this calculation as these effects are likely not small [48].

π^a : Eight pseudo-scalar mesons π^a corresponding to the broken axial flavour generators. As colour singlets these remain as propagating degrees of freedom in both QCD and NJL models. These have the quantum numbers of pions, kaons and the eta and transform as an octet under the unbroken symmetry.

ϕ^a : Eight scalar bosons ϕ^a corresponding to the broken coloured generators. These are eaten by the gauge bosons in QCD and are removed from the low-energy theory. This gives masses to eight of the gauge bosons and decouples them from low-energy physics. In the NJL model these bosons still remain as low-energy degrees of freedom, but decouple from the colour singlet physics when one properly enforces colour neutrality.

There are additional fields and effects that should be considered as part of a complete low-energy theory, but that we neglect:

1. The appropriately “rotated electromagnetic field” associated with the unbroken $U(1)_{\bar{Q}}$ symmetry remains massless. Both the CFL and CFLK⁰ states remain neutral with respect to this field, however, and we do not explicitly include it in our formulation.
2. The leptons are not strictly massless, but the electron and muon are light enough to consider in the low-energy physics. In particular, they contribute to the charge density in the presence of an electric chemical potential and at finite temperature. In this paper, leptonic excitations play no role since we consider only $T = 0$ and both CFL and CFLK⁰ quark matter is electrically neutral for $\mu_e = 0$. The leptons play an implicit role in fixing $\mu_{\bar{Q}}$ such that $\mu_e = 0$ in both insulating phases.

To be explicit, we relate all of the dimensional physical fields H , η' , ϕ^a and π^a to the phase angles through their decay constants: $H = f_H \tilde{H}$, $\eta' = f_{\eta'} \tilde{\eta}'$, $\phi^a = f_\phi \tilde{\phi}^a$, and $\pi^a = f_\pi \tilde{\pi}^a$. The two $U(1)$ phases angles have a slightly different normalization because of the normalization of the generators. This normalization is chosen to match the kinetic terms in the original theory and matches [22, 23]: $\tilde{\eta}' = \sqrt{6}(\theta_R - \theta_L)$, and $\tilde{H}' = \sqrt{6}(\theta_R + \theta_L)$. The realization of these transformations in the microscopic theory is

$$\psi \rightarrow \exp \left\{ i \left[\frac{-\tilde{H}\mathbf{1} - \tilde{\eta}'\gamma_5}{2\sqrt{6}} + \tilde{\phi}^a \mathbf{r}^a + \tilde{\pi}^a \mathbf{f}_A^a \right] \right\} \psi \quad (31)$$

where

$$\mathbf{f}_{R,L}^a = (\mathbf{1} \pm \gamma_5) \otimes (-\lambda_a^*) \otimes \mathbf{1}/2, \quad (32a)$$

$$\mathbf{c}^a = \mathbf{1} \otimes \mathbf{1} \otimes \lambda_a, \quad (32b)$$

$$\mathbf{f}_A^a = \mathbf{f}_R^a - \mathbf{f}_L^a = \gamma_5 \otimes (-\lambda_a^*) \otimes \mathbf{1}, \quad (32c)$$

$$\mathbf{f}_V^a = \mathbf{f}_R^a + \mathbf{f}_L^a = \mathbf{1} \otimes (-\lambda_a^*) \otimes \mathbf{1}, \quad (32d)$$

$$\mathbf{r}^a = (\mathbf{f}_V^a - \mathbf{c}^a)/2 \quad (32e)$$

and the corresponding realization in the effective theory is

$$\mathbf{X} = \exp \{-i\tilde{\pi}^a \lambda_a\} \exp \{i\tilde{\phi}^a \lambda_a\}, \quad (33a)$$

$$\mathbf{Y} = \exp \{i\tilde{\pi}^a \lambda_a\} \exp \{i\tilde{\phi}^a \lambda_a\}, \quad (33b)$$

$$A = \exp \left\{ 2i\tilde{\eta}'/\sqrt{6} \right\}, \quad (33c)$$

$$V = \exp \left\{ 2i\tilde{H}/\sqrt{6} \right\}, \quad (33d)$$

$$\Sigma = \exp \{-2i\tilde{\pi}^a \lambda_a\}. \quad (33e)$$

B. Power Counting

In addition to Λ_{QCD} which separates the three light quarks from the heavy quarks, there are two primary scales in high-density QCD: the quark chemical potential μ_q and the gap Δ . In the NJL model there is also a cutoff and the coupling constant: these are related by the gap equation when one holds μ and Δ fixed and the qualitative physics is not extremely sensitive to the remaining renormalization parameter.

Our low-energy theory is an expansion in the energy/momentum of the Goldstone fields. Thus, the expansion is in powers of the derivatives with respect to the scales μ and Δ . In this paper, we shall only consider leading order terms: Systematic expansions have been discussed elsewhere (see for example [65]).

C. Kinetic Terms

To construct the low-energy theory we follow [18] and introduce coloured currents

$$\mathbf{J}_X^\mu = \mathbf{X}^\dagger \partial_{(v)}^\mu \mathbf{X} \rightarrow \mathbf{C} \mathbf{J}_X^\mu \mathbf{C}^\dagger,$$

$$\mathbf{J}_Y^\mu = \mathbf{Y}^\dagger \partial_{(v)}^\mu \mathbf{Y} \rightarrow \mathbf{C} \mathbf{J}_Y^\mu \mathbf{C}^\dagger,$$

$$\mathbf{J}_\pm^\mu = \mathbf{J}_X^\mu \pm \mathbf{J}_Y^\mu \rightarrow \mathbf{C} \mathbf{J}_\pm^\mu \mathbf{C}^\dagger.$$

In the presence of a finite density, we no longer have manifest Lorentz invariance and must allow for additional constants into our spatial derivatives

$$\partial_{(v)}^\mu = (\partial^0, v\partial^i)$$

to account for the differing speeds of sound. This paper will be concerned with static properties, so we can neglect these. In principle, one must also match these coefficients v . In QCD this matching, along with other coefficients, has been made with perturbative calculations at asymptotic densities [22, 23]. Our theory and states still maintain rotational invariance. Thus, to lowest-order we have [18]

$$\begin{aligned} \mathcal{L}_{\text{eff}} &= \mathcal{L}_{\eta'} + \mathcal{L}_\Sigma + \mathcal{L}_H + \mathcal{L}_\phi + \dots, \\ &= \frac{3f_{\eta'}^2}{4} \partial_{(v_{\eta'})}^\mu A^\dagger \partial_{(v_{\eta'})\mu} A - \frac{f_\pi^2}{4} \text{Tr}[\mathbf{J}_-^\mu \mathbf{J}_{-\mu}] + \\ &\quad + \frac{3f_H^2}{4} \partial_{(v_H)}^\mu V^\dagger \partial_{(v_H)\mu} V - \frac{f_\phi^2}{4} \text{Tr}[\mathbf{J}_+^\mu \mathbf{J}_{+\mu}] + \dots, \\ &= \frac{1}{2} \partial_{(v_{\eta'})}^\mu \eta' \partial_{(v_{\eta'})\mu} \eta' + \frac{1}{2} \partial_{(v_\pi)}^\mu \pi^a \partial_{(v_\pi)\mu} \pi^a + \\ &\quad + \frac{1}{2} \partial_{(v_H)}^\mu H \partial_{(v_H)\mu} H + \frac{1}{2} \partial_{(v_\phi)}^\mu \phi^a \partial_{(v_\phi)\mu} \phi^a + \dots \end{aligned}$$

The neglected terms are of higher order in the derivative expansion. Note that our normalizations have been chosen so that this expression is canonically normalized to quadratic order in terms of the dimensionful fields.

The division of \mathcal{L}_{eff} is natural [18] because it separates out the colour singlets. \mathcal{L}_Σ depends only on Σ for example:

$$\mathcal{L}_\Sigma = -\frac{f_\pi^2}{4} \text{Tr}[\mathbf{J}_-^\mu \mathbf{J}_{-\mu}] = \frac{f_\pi^2}{4} \text{Tr}[\partial_{(v_\pi)}^\mu \Sigma^\dagger \partial_{(v_\pi)\mu} \Sigma].$$

Thus, with the exceptions noted above, the lowest-order low-energy effective theory of massless $N_f = 3$ QCD is

$$\mathcal{L}_{\text{QCD}} = \mathcal{L}_\Sigma + \mathcal{L}_H + \mathcal{L}_{\eta'} + \dots \quad (34)$$

whereas the NJL model proper must also include \mathcal{L}_ϕ .

D. Perturbations

We shall now consider two types of perturbations: chemical potentials and quark masses. To deal with these perturbations, we note that they enter the microscopic Lagrangian as

$$\mathcal{L}_{\text{SB}} = \psi_L^\dagger \boldsymbol{\mu}^L \psi_L + \psi_R^\dagger \boldsymbol{\mu}^R \psi_R + \psi_R^\dagger \mathbf{M} \psi_L + \psi_L^\dagger \mathbf{M}^\dagger \psi_R.$$

These terms break the original symmetries of the theory, but one can restore these symmetries by imparting the following spurion transformations to the masses and chemical potentials

$$\mathbf{M} \rightarrow \pm(\mathbf{F}_R^* \otimes \mathbf{C})\mathbf{M}(\mathbf{F}_L^* \otimes \mathbf{C})^\dagger e^{-i(\theta_R - \theta_L)}, \quad (35a)$$

$$\mu^L \rightarrow (\mathbf{F}_L^* \otimes \mathbf{C})\mu^L(\mathbf{F}_L^* \otimes \mathbf{C})^\dagger, \quad (35b)$$

$$\mu^R \rightarrow (\mathbf{F}_R^* \otimes \mathbf{C})\mu^R(\mathbf{F}_R^* \otimes \mathbf{C})^\dagger. \quad (35c)$$

The transformation $\mathbf{M} \rightarrow -\mathbf{M}$ preserves the residual Z_2 symmetries. This prevents odd powers of the mass terms from appearing in the chiral effective theory. In particular, the linear term dominant in the vacuum is forbidden, resulting in an inverse mass-ordering of the mesons [22, 23] with the kaon being the lightest particle at high density.

All these symmetries must be restored in the effective theory: we are only allowed to couple these parameters to the fields in ways that preserve the global symmetries. To lowest-order, this greatly limits the possible terms in the effective theory.

In the case of the chemical potentials, we can go one step further by noting that the perturbations always appears in combination with the time derivative

$$\mathcal{L} = \psi^\dagger(i\partial_0 + \mu)\psi + \dots \quad (36)$$

One can thus promote the chemical potentials to a temporal component of a spurion gauge field and render the symmetries local in time:

$$\mu \rightarrow (\mathbf{F}^* \otimes \mathbf{C})(\mu + i\partial_0)(\mathbf{F}^* \otimes \mathbf{C})^\dagger. \quad (37)$$

The effective theory must also maintain these local symmetries. One concludes that the chemical potential perturbations can only appear through the introduction of covariant derivatives in the effective theory. In particular, consider adding independent colour and flavour chemical potential terms:

$$\mu^{L,R} = \mu_{L,R} \mathbf{1} \otimes \mathbf{1} + \mu_F^{L,R} \otimes \mathbf{1} + \mathbf{1} \otimes \mu_C \quad (38)$$

where μ_F and μ_C are traceless 3×3 matrices. From these we may construct the following quantities that transform covariantly:

$$\nabla_0 \mathbf{X} = \partial_0 \mathbf{X} + i[\mu_F^L]^* \mathbf{X} + i\mathbf{X} \mu_C, \quad (39a)$$

$$\nabla_0 \mathbf{Y} = \partial_0 \mathbf{Y} + i[\mu_F^R]^* \mathbf{Y} + i\mathbf{Y} \mu_C, \quad (39b)$$

$$\nabla_0 \Sigma = \partial_0 \Sigma + i[\mu_F^L]^* \Sigma - i\Sigma[\mu_F^R]^T, \quad (39c)$$

$$\nabla_0 V = (\partial_0 + 2i\mu_V) V, \quad (39d)$$

$$\nabla_0 A = (\partial_0 + 2i\mu_A) A, \quad (39e)$$

where $\mu_V = \mu_R + \mu_L$ is a small adjustment of the baryon chemical potential $\mu_B/3$ and $\mu_A = \mu_R - \mu_L$ is the “axial baryon” chemical potential. For the rest of this paper, we shall only consider vector chemical potentials that are real and symmetric: $\mu_F^{L,R} = \mu_F = \mu_F^* = \mu_F^\dagger$ etc. With

these restrictions, the static potential in the effective theory is

$$V = \frac{f_\pi^2}{2} \text{Tr}[\Sigma^\dagger \mu_F \Sigma \mu_F - \mu_F^2] - 3f_H^2[\mu_V]^2 - 3f_{\eta'}^2[\mu_A]^2 + \frac{f_\phi^2}{4} \text{Tr} \left[\left(\mathbf{X}^\dagger \mu_F \mathbf{X} + \mathbf{Y}^\dagger \mu_F \mathbf{Y} + 2\mu_C \right)^2 \right] + \dots \quad (40)$$

to lowest-order. The terms omitted include terms of higher order in the perturbation and small corrections due to the explicit violation of the “local” spurion symmetries by the cutoff.

E. Charge Neutrality

As discussed in [45, 54, 55], the gauge-invariance of QCD implies that homogeneous states must be colour neutral. Non-zero static colour sources $\mathbf{A}_C^0(\vec{\mathbf{p}}=0)$ cancel the tadpole diagrams ensuring neutrality. These sources enter the NJL calculation as Lagrange multipliers to enforce neutrality.

One can see explicitly how these arise in the context of the effective theory. The gauge fields effect the local symmetry and thus couple through the derivatives in exactly the same way as the spurion coloured chemical potentials: $\mu_C \propto g_s \mathbf{A}_C^0$. Enforcing gauge-invariance induces an effective coloured chemical potential that makes (40) stationary with respect to variations of the gauge field, and thus equivalently, with respect to traceless variations of μ_C . Thus, we see that, to lowest-order [18, 54, 55]

$$\mu_C = -\frac{1}{2} \left(\mathbf{X}^\dagger \mu_F \mathbf{X} + \mathbf{Y}^\dagger \mu_F \mathbf{Y} \right). \quad (41)$$

Inserting this into the (40), and considering only traceless perturbations, we see that the colour dependence drops out of the effective theory and we are left with the static effective potential involving only the colour singlet fields:

$$V = \frac{f_\pi^2}{2} \text{Tr}[\Sigma^\dagger \mu_F \Sigma \mu_F - \mu_F^2] + \dots \quad (42)$$

In order to reproduce the physics of this in the NJL model, however, we must remove the coloured degrees of freedom. This is done by introducing colour chemical potentials to the NJL model as Lagrange multipliers and using them to impose colour neutrality [45, 54, 55]. This removes the colour dependence in the NJL model to all orders in the same way as it removes the colour dependence in (41) to lowest-order. (In general, it is not sufficient to impose colour neutrality: one must also project onto colour singlet states (as well as states of definite baryon number). This projection is important for small systems, but likely has negligible cost for thermodynamically large systems such as neutron stars. See [66] for an explicit demonstration of this in the two-flavour case.)

The quarks also couple to the photon, and so we also must enforce electric neutrality. Enforcing electromagnetic gauge-invariance will likewise induce an electric

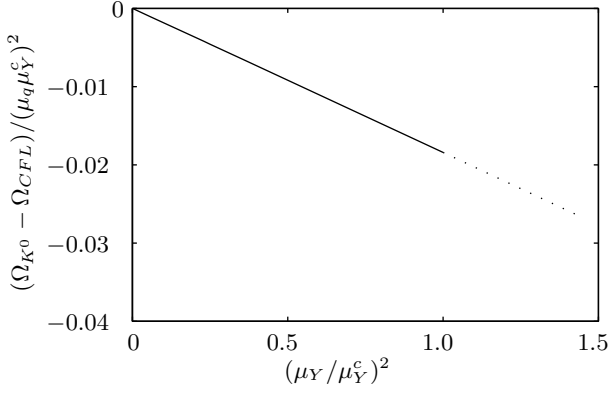


FIG. 7: Numerical difference in energy densities between the kaon-condensed CFLK⁰ state and the CFL state at finite hypercharge potential μ_Y obtained from our microscopic NJL calculation. The units are scaled in terms of the quark chemical potential $\mu_q = 500$ MeV and the critical hypercharge chemical potential $\mu_Y^c = 25$ MeV. The quantities plotted were chosen so that the relationship will be linear if our calculation agrees with the effective theory result (45). The slope of the line is $m = -f_\pi^2/2\mu_q^2 \approx -0.018$ from which we can determine the effective theory parameter $f_\pi \approx 0.19\mu_q$. This is in good numerical agreement with the perturbative QCD result $f_\pi \approx 0.209\mu_q$ [22, 23]. The dashed extension shows the comparison between the CFLK⁰ potential and the CFL potential, but beyond 1.0, the CFL becomes the gCFL and the energy dependence changes. We have not calculated the gCFL potential in this paper, but plot this extension to emphasize that the CFLK⁰ persists beyond the CFL/gCFL transition point at 1.0.

chemical potential μ_e that ensures electric neutrality. It turns out that both the CFL and the CFLK⁰ quark matter are neutral under a residual charge \tilde{Q} (both are \tilde{Q} insulators). This means that one has some freedom in choosing the chemical potentials used to enforce neutrality. In particular, prior to the onset of gapless modes, one may choose these combinations so that $\mu_e = 0$. This is naturally enforced by including charged leptons in the calculation.

Once a charged excitation becomes gapless, the material becomes a conductor and a non-zero μ_e is required to enforce neutrality. The phase transition to the gCFL and gCFLK⁰ is defined by exactly such a charged excitation. In this paper, we shall only consider the insulating phases, and thus simply set $\mu_e = 0$. For further discussions of the metal/insulator properties of the CFL and gCFL we refer the reader to [37, 39, 40].

F. Kaon Condensation

We are now in a position to argue for the existence of a kaon-condensed state. Consider performing an axial K⁰ rotation on the parity-even CFL state. This is effected using (31) in the microscopic theory and using (33) in the effective theory with the parameter $\tilde{\pi}^6 = \theta$. Such a

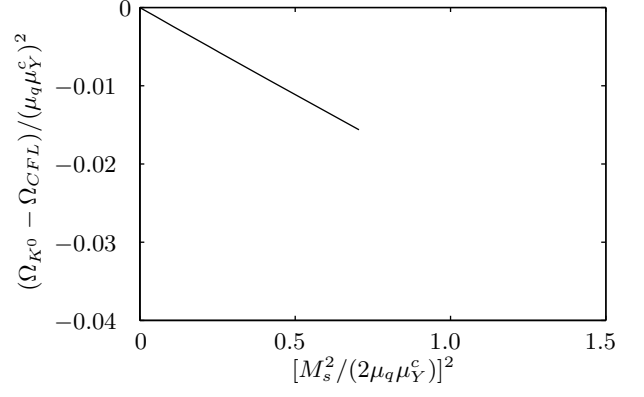


FIG. 8: Numerical difference in energy densities between the kaon-condensed CFLK⁰ state and the CFL state at finite strange quark mass m_s obtained from our microscopic NJL calculation. The units are scaled in terms of the renormalized quark chemical potential $\mu_q \approx 500$ MeV and the critical hypercharge chemical potential $\mu_Y^c = 25$ MeV to facilitate comparison with Figure 7 and to emphasize the linear relationship implicit in (47). The slope of the line is $m \approx -f_\pi^2/2\mu_q^2 \approx -0.028$ which gives an effective $f_\pi \approx 0.21\mu_q$ which is consistent with our previous results. In comparison with Figure 7, the CFL→gCFL transition occurs somewhat earlier because the gap parameters are reduced with increasing strange quark mass. The curve cannot be extended as in Figure 7 because the free-energy of the CFL is no longer a constant as it was with a hypercharge perturbation.

state is now described by

$$\Sigma = e^{2i\theta\lambda_6} = \begin{pmatrix} 1 & & \\ & \cos(\theta) & i\sin(\theta) \\ & i\sin(\theta) & \cos(\theta) \end{pmatrix}. \quad (43)$$

In the presence of a hypercharge chemical potential, the effective potential becomes [31, 32, 33]

$$V(\theta) = \frac{f_\pi^2 \mu_Y^2}{2} (\cos^2(\theta) - 1) + \dots \quad (44)$$

We see that this has a minimum for $\theta = \pm\pi/2$: this is the state with maximal K⁰ condensation. We can also directly compute the difference in the thermodynamic potential densities between the CFL state and the CFLK⁰ state:

$$\Omega_{\text{CFLK}^0} - \Omega_{\text{CFL}} = -\frac{f_\pi^2 \mu_Y^2}{2}. \quad (45)$$

Armed with this relationship, we can now turn to the microscopic calculation and determine the coefficient f_π . In Figure 7 we plot our numerical results so that the linear relationship (45) is evident. From the slope of the relationship we find that

$$f_\pi \approx 0.19\mu_q. \quad (46)$$

We note that this is in good numerical agreement with the perturbative QCD result [22, 23] of $f_\pi = 0.209\mu_q$.

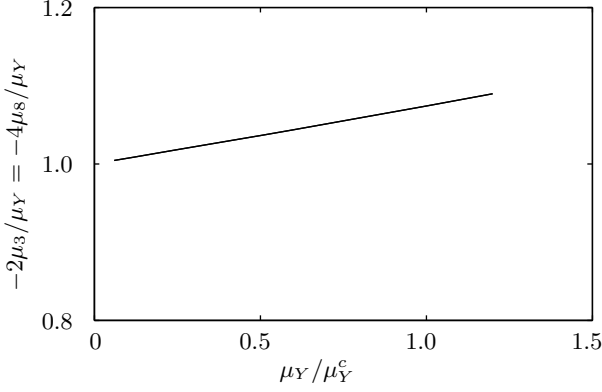


FIG. 9: Chemical potentials required by the NJL model to enforce colour neutrality in the CFLK⁰ phase with finite hypercharge chemical potentials. Note that the effective theory relationship (50) is satisfied from small chemical potentials. The linear deviation seen here reflects the missing terms in the effective theory that are of higher order in the perturbation μ_Y with a linear deviation here corresponds to μ_Y^2 terms missing in (50).

This striking agreement between two very different models arises from the fact that this coefficient is not very sensitive to the effects of the cutoff (which is different in the two theories) and gives encouraging support to the use of the NJL model to study QCD.

The equivalent relationship in the case of a strange quark mass requires one to include mass terms in the effective theory (see for example [30]), but the leading order effect can be determined by using the “effective” strange quark chemical potential $\mu_Y \approx M_s^2/(2\mu_q)$ that follows from (3):

$$\Omega_{\text{CFLK}^0} - \Omega_{\text{CFL}} = -\frac{f_\pi^2}{2} \left(\frac{M_s^2}{2\mu_q} \right)^2. \quad (47)$$

It is important here to note, however, that the strange quark mass affects the solution in such a way that the gap parameters change and self-energy corrections modify the quark chemical potential and the constituent quark mass. It is the renormalized parameters that appear in this relation and in the perturbative QCD result. Thus, as a function of the bare parameter m_s , we have $M_s \propto m_s$ and $\mu_q - \mu_s \propto m_s^2$. Thus, we should see a linear relationship between $\Omega_{\text{CFLK}^0} - \Omega_{\text{CFL}}$ and M_s^4 . We plot this relationship in Figure 8 and extract the slope which gives the relationship $f_\pi \approx 0.21\mu_q$. This is in qualitative agreement with our previous result. The slight numerical disagreement is due to effects of the strange quark mass that are not captured by the chemical potential shift (3).

We pause here to point out a discrepancy between our results and similar work by Buballa [67]. Our results shown in Figure 8 suggests that kaon condensation occurs for all values of m_s in this simple model with $m_u = m_d = 0$ whereas Buballa finds that kaon condensation is only favoured for m_s sufficiently large. If the

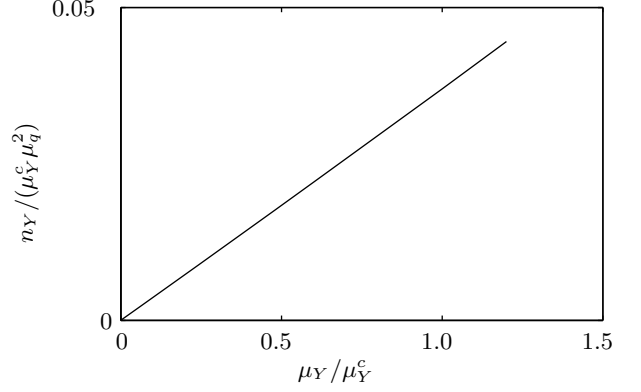


FIG. 10: Hypercharge density of the CFLK⁰ state in the presence of a hypercharge chemical potential μ_Y as obtained from our microscopic NJL model calculation. The units are scaled as in Figure 7 so that the relationship will be linear if the NJL model calculation agrees with the effective theory prediction (51). By determining the slope of this relationship we have another way of determining the coefficient f_π in the effective theory. The slope is $f_\pi^2/\mu_q^2 \approx 0.037$ which agrees with our previous determination of $f_\pi \approx 0.19\mu_q$.

chemical potential shift were the only effect of a strange quark mass, then this would be inconsistent with (40). This is not, however, the correct expansion. Instead, one has, for maximal kaon condensation and $m_u = m_d = 0$:

$$\Omega_{\text{CFLK}^0} - \Omega_{\text{CFL}} = -(4a_6 + a_8)m_s^2 - cm_s^4 + \mathcal{O}(m_s^6). \quad (48)$$

A proper discussion of this is beyond the scope of this paper, but will be discussed elsewhere [68]. The term with coefficient c should be identified with the leading order contribution from (3); the term with coefficient a_6 arises from the sextet gap contribution Δ_6 and is discussed in [49]; the term with coefficient a_8 is of higher order in perturbative QCD and so is usually neglected [22, 23, 30].

Thus, Buballa’s results are consistent with the effective theory. The discrepancy is due to a different choice of parameters $\Delta \sim 100$ MeV and $\Lambda = 600$ MeV compared with our parameters $\Delta \sim 25$ MeV and $\Lambda = 800$ MeV. With the large gap, one is further from the perturbative QCD regime and the quadratic term appears to play a significant role. In our analysis, the term $-(4a_6 + a_8)m_s^2$ is small compared with the cm_s^4 term. Using Buballa’s parameters, however, we qualitatively reproduce his results. A further discussion of these effects will be presented shortly [68].

There are a couple of other consequences that follow directly from the effective theory. One is the value of the coloured chemical potentials required to enforce neutrality. In our microscopic model, we have fixed the gauge (unitary gauge) by setting $\mathbf{X} = \mathbf{Y}^\dagger = \sqrt{\Sigma}$ for the axial rotations. The CFL state has $\mathbf{X} = \mathbf{Y} = \mathbf{1}$ while the

CFLK⁰ state has

$$\mathbf{X} = \mathbf{Y}^\dagger = \frac{1}{\sqrt{2}} \begin{pmatrix} \sqrt{2} & & \\ & 1 & i \\ & i & 1 \end{pmatrix}. \quad (49)$$

From (41) we have the following relationships required to enforce neutrality [54]

$$\mu_8 = -\mu_Y, \quad \mu_3 = 0, \quad (\text{CFL}), \quad (50a)$$

$$\mu_8 = -\frac{1}{4}\mu_Y, \quad \mu_3 = -\frac{1}{2}\mu_Y, \quad (\text{CFLK}^0). \quad (50b)$$

We plot these relationships in Figure 9. Note that they only hold for small perturbations where the effective theory is valid: this plot also demonstrates a departure from the lowest-order effective theory as the perturbation is increased.

As a final demonstration of the effective theory, we calculate the hypercharge density. This is obtained by varying the thermodynamic potential with respect to the hypercharge chemical potential:

$$n_Y = -\frac{\partial \Omega}{\partial \mu_Y} \approx -f_\pi^2 \mu_Y (\cos^2(\theta) - 1). \quad (51)$$

There should be no hypercharge density in the CFL state and a density of $n_Y = f_\pi^2 \mu_Y$ in the CFLK⁰ state. Indeed, the CFL supports no hypercharge density with $n_u = n_d = n_s$. The hypercharge density of the CFLK⁰ phase is shown in Figure 10 and provides another method of extracting $f_\pi = 0.19\mu_q$.

G. A Note on the Meaning of $V(\theta)$

We make a few remarks here about the meaning of the effective potential $V(\theta)$. In particular, one might be tempted to try and compute the functional form of $V(\theta)$ in the microscopic theory to facilitate matching with the effective theory. Such an approach will generally fail because one is allowed to pick an arbitrary parametrization of the Goldstone fields as long as they leave the kinetic terms unaltered [69, 70]. Physical quantities must be invariant under this change of parametrization: thus the spectrum about the minimum, densities, and energy differences are reasonable quantities to compare in each theory. The general form of the effective potential away from the stationary points, however, is rather arbitrary.

As an example: consider starting with the parity even CFL state in the presence of a finite μ_Y . This state corresponds to a stationary point of the effective potential and is a self-consistent solution to the gap equations. One can then form a continuum of “kaon rotated” states $|\theta\rangle$ by applying the broken symmetry generators to this state. One might expect to find $V(\theta)$ by computing the energy of these states, but instead one finds an expression that is only valid locally about the stationary point. The reason is twofold: First, there is not a unique “kaon

rotated” state $|\theta\rangle$. This state has many other parameters corresponding to other “directions” (such as the gap parameters Δ , the chemical potential corrections etc.) The only way to uniquely determine these is to solve the gap equations, and these only have well-defined solutions at stationary points. Second, the generators of the pseudo-Goldstone bosons in the presence of perturbations are not the same as the generators of the true Goldstone bosons in the unbroken model: the pseudo-Goldstone bosons have some admixture of these other “directions”.

This becomes even more evident when you analyze the CFLK⁰ state with a large perturbation: one can try to “undo” the kaon rotation by applying the appropriate symmetry generators to minimize the parity violating condensates, but one finds that there is no way to do this. One must also transform the other parameters in order convert a CFLK⁰ state back to a parity even CFL state.

VI. CONCLUSION

We have explicitly found self-consistent solutions within a microscopic NJL model exhibiting the feature of kaon condensation in a colour-flavour-locked state. Using these solutions, we have demonstrated that by properly enforcing gauge neutrality, one can remove the extraneous coloured degrees of freedom from the NJL model and effectively model kaon condensation in high-density QCD. In particular, the microscopic calculations can be matched onto the low-energy effective theory of QCD. We determined $f_\pi = 0.19\mu_q$ which is in good numerical agreement with the perturbative QCD result.

Furthermore, our solutions are fully self-consistent: no approximations have been made beyond the mean-field approximation and restricting our attention to isotropic and homogeneous states. We find that our results agree qualitatively with both the expected properties of the CFLK⁰ phase based on effective theory calculations, and with the previous numerical calculations of the CFL/gCFL transition.

Quantitatively we find that the phase transitions occur at slightly smaller parameter values than previously found in the literature. Concerning the CFL/gCFL transition, we find that the gap parameters are reduced by a few percent compared with those presented in [40], and subsequently, the critical M_s is also a few percent lower. Concerning the CFLK⁰/gCFLK⁰ transition, we find that the transition occurs about a factor of 1.2 higher than the CFL/gCFL transition. This is in qualitative agreement but quantitative disagreement with the factor of 4/3 calculated in [34].

The next step is to use this microscopic model to determine the phase structure of high-density QCD in the region where the gapless modes appear. We suspect that the gCFLK⁰ state will survive somewhat longer than the gCFL state on account of its lower condensation energy,

but a quantitative comparison is required. Extrapolation to finite temperature is also a trivial extension in our formalism.

A somewhat more challenging direction is to consider the effects of instantons and finite up and down quark masses and investigate other forms of meson condensation. Preliminary investigations indicate, however, that the number of parameters required to close the gap equations in the presence of arbitrary meson rotations may be prohibitively large to continue with fully self-consistent calculations. This should still be tractable with carefully made approximations.

VII. ACKNOWLEDGEMENTS

I would like to thank K. Rajagopal and F. Wilczek for suggesting this problem, and P. Bedaque, K. Fukushima,

D. K. Hong, D. Kaplan, C. Kouvaris, J. Kundu, M. J. Savage, T. Schäfer, I. Shovkovy, I. Stewart, and A. R. Zhitnitsky for useful discussions. Related work has been done independently by M. Buballa [67] and I am grateful to him for postponing his preprint submission while the first version of this work was completed. This work is supported in part by funds provided by the U.S. Department of Energy (D.O.E.) under cooperative research agreement #DF-FC02-94ER40818.

-
- [1] B. C. Barrois, Nucl. Phys. **B129**, 390 (1977).
 - [2] S. Frautschi, Proceedings of workshop on hadronic matter at extreme density, Erice, 1978, Proceedings of workshop on hadronic matter at extreme density.
 - [3] B. C. Barrois, *Non-perturbative effects in dense quark matter*, PhD thesis, Caltech, 1979, UMI 79-04847-mc.
 - [4] D. Bailin and A. Love, Phys. Rept. **107**, 325 (1984).
 - [5] M. Alford, K. Rajagopal, and F. Wilczek, Phys. Lett. **B422**, 247 (1998), arXiv:hep-ph/9711395.
 - [6] R. Rapp, T. Schafer, E. V. Shuryak, and M. Velkovsky, Phys. Rev. Lett. **81**, 53 (1998), arXiv:hep-ph/9711396.
 - [7] M. Alford, K. Rajagopal, and F. Wilczek, Nucl. Phys. **B537**, 443 (1999), arXiv:hep-ph/9804403.
 - [8] D. T. Son, Phys. Rev. **D59**, 094019 (1999), arXiv:hep-ph/9812287.
 - [9] D. K. Hong, Nucl. Phys. **B582**, 451 (2000), arXiv:hep-ph/9905523.
 - [10] N. J. Evans, J. Hormuzdiar, S. D. H. Hsu, and M. Schwetz, Nucl. Phys. **B581**, 391 (2000), arXiv:hep-ph/9910313.
 - [11] K. Rajagopal and F. Wilczek, (2000), arXiv:hep-ph/0011333.
 - [12] M. G. Alford, Ann. Rev. Nucl. Part. Sci. **51**, 131 (2001), arXiv:hep-ph/0102047.
 - [13] G. Nardulli, Riv. Nuovo Cim. **25N3**, 1 (2002), arXiv:hep-ph/0202037.
 - [14] S. Reddy, Acta Phys. Polon. **B33**, 4101 (2002), arXiv:nucl-th/0211045.
 - [15] T. Schafer, (2003), arXiv:hep-ph/0304281.
 - [16] T. Schafer, Nucl. Phys. **B575**, 269 (2000), arXiv:hep-ph/9909574.
 - [17] I. A. Shovkovy and L. C. R. Wijewardhana, Phys. Lett. **B470**, 189 (1999), arXiv:hep-ph/9910225.
 - [18] R. Casalbuoni and R. Gatto, Phys. Lett. **B464**, 111 (1999), arXiv:hep-ph/9908227.
 - [19] D. K. Hong, Phys. Lett. **B473**, 118 (2000), arXiv:hep-ph/9812510.
 - [20] S. R. Beane, P. F. Bedaque, and M. J. Savage, Phys. Lett. **B483**, 131 (2000), arXiv:hep-ph/0002209.
 - [21] V. A. Miransky, I. A. Shovkovy, and L. C. R. Wijewardhana, Phys. Lett. **B468**, 270 (1999), arXiv:hep-ph/9908212.
 - [22] D. T. Son and M. A. Stephanov, Phys. Rev. **D61**, 074012 (2000), arXiv:hep-ph/9910491, Erratum: [23].
 - [23] D. T. Son and M. A. Stephanov, Phys. Rev. **D62**, 059902(E) (2000), arXiv:hep-ph/0004095, Erratum to [22].
 - [24] M. Rho, A. Wirzba, and I. Zahed, Phys. Lett. **B473**, 126 (2000), arXiv:hep-ph/9910550.
 - [25] D. K. Hong, T. Lee, and D.-P. Min, Phys. Lett. **B477**, 137 (2000), arXiv:hep-ph/9912531.
 - [26] C. Manuel and M. H. G. Tytgat, Phys. Lett. **B479**, 190 (2000), arXiv:hep-ph/0001095.
 - [27] M. Rho, E. V. Shuryak, A. Wirzba, and I. Zahed, Nucl. Phys. **A676**, 273 (2000), arXiv:hep-ph/0001104.
 - [28] K. Zarembo, Phys. Rev. **D62**, 054003 (2000), arXiv:hep-ph/0002123.
 - [29] D. K. Hong, Phys. Rev. **D62**, 091501(R) (2000), arXiv:hep-ph/0006105.
 - [30] T. Schafer, Phys. Rev. **D65**, 074006 (2002), arXiv:hep-ph/0109052.
 - [31] T. Schafer, Phys. Rev. Lett. **85**, 5531 (2000), arXiv:nucl-th/0007021.
 - [32] P. F. Bedaque and T. Schafer, Nucl. Phys. **A697**, 802 (2002), arXiv:hep-ph/0105150.
 - [33] D. B. Kaplan and S. Reddy, Phys. Rev. **D65**, 054042 (2002), arXiv:hep-ph/0107265.
 - [34] A. Kryjevski and D. Yamada, Phys. Rev. **D71**, 014011 (2005), arXiv:hep-ph/0407350.
 - [35] Y. Nambu and G. Jona-Lasinio, Phys. Rev. **122**, 345 (1961).
 - [36] Y. Nambu and G. Jona-Lasinio, Phys. Rev. **124**, 246 (1961).
 - [37] M. Alford, C. Kouvaris, and K. Rajagopal, Phys. Rev. Lett. **92**, 222001 (2004), arXiv:hep-ph/0311286.
 - [38] M. Alford, C. Kouvaris, and K. Rajagopal, Phys. Rev. **D71**, 054009 (2005), arXiv:hep-ph/0406137.
 - [39] S. B. Ruster, I. A. Shovkovy, and D. H. Rischke, Nucl. Phys. **A743**, 127 (2004), arXiv:hep-ph/0405170.
 - [40] K. Fukushima, C. Kouvaris, and K. Rajagopal, Phys.

- Rev. **D71**, 034002 (2005), arXiv:hep-ph/0408322.
- [41] A. Kryjevski and T. Schafer, Phys. Lett. **B606**, 52 (2005), arXiv:hep-ph/0407329.
 - [42] A. Barducci, R. Casalbuoni, G. Pettini, and L. Ravagli, Phys. Rev. **D71**, 016011 (2005), arXiv:hep-ph/0410250.
 - [43] T. Schafer and F. Wilczek, Phys. Rev. Lett. **82**, 3956 (1999), arXiv:hep-ph/9811473.
 - [44] M. Alford, J. Berges, and K. Rajagopal, Nucl. Phys. **B571**, 269 (2000), arXiv:hep-ph/9910254.
 - [45] M. Alford and K. Rajagopal, JHEP **06**, 031 (2002), arXiv:hep-ph/0204001.
 - [46] R. Rapp, T. Schafer, E. V. Shuryak, and M. Velkovsky, Annals Phys. **280**, 35 (2000), arXiv:hep-ph/9904353.
 - [47] D. T. Son, M. A. Stephanov, and A. R. Zhitnitsky, Phys. Lett. **B510**, 167 (2001), arXiv:hep-ph/0103099.
 - [48] T. Schafer, Phys. Rev. **D65**, 094033 (2002), arXiv:hep-ph/0201189.
 - [49] A. Kryjevski, D. B. Kaplan, and T. Schafer, Phys. Rev. **D71**, 034004 (2005), arXiv:hep-ph/0404290.
 - [50] K. Rajagopal and F. Wilczek, Phys. Rev. Lett. **86**, 3492 (2001), arXiv:hep-ph/0012039.
 - [51] P. F. Bedaque, Nucl. Phys. **A697**, 569 (2002), arXiv:hep-ph/9910247.
 - [52] M. G. Alford, J. A. Bowers, and K. Rajagopal, J. Phys. **G27**, 541 (2001), arXiv:hep-ph/0009357.
 - [53] J. Kundu and K. Rajagopal, Phys. Rev. **D65**, 094022 (2002), arXiv:hep-ph/0112206.
 - [54] A. Kryjevski, Phys. Rev. **D68**, 074008 (2003), arXiv:hep-ph/0305173.
 - [55] A. Gerhold and A. Rebhan, Phys. Rev. **D68**, 011502(R) (2003), arXiv:hep-ph/0305108.
 - [56] R. P. Feynman, *Statistical Mechanics* Advanced Book Classics, 2 ed. (Perseus Books, Reading, Massachusetts, 1998).
 - [57] M. M. Forbes, *Fermionic Superfluids: From Cold Atoms to High Density QCD. Gapless (Breached Pair) Superfluidity and Kaon Condensation*, PhD thesis, MIT, 2005.
 - [58] C. G. Broyden, Math. Comput. **19**, 577 (1965).
 - [59] J. E. Dennis and R. B. Schnabel, *Numerical Methods for Unconstrained Optimization and Nonlinear Equations* (Prentice-Hall, Englewood Cliffs, N.J., 1983).
 - [60] M. G. Alford, J. Berges, and K. Rajagopal, Nucl. Phys. **B558**, 219 (1999), arXiv:hep-ph/9903502.
 - [61] M. Buballa and M. Oertel, Nucl. Phys. **A703**, 770 (2002), arXiv:hep-ph/0109095.
 - [62] D. K. Hong, M. Rho, and I. Zahed, Phys. Lett. **B468**, 261 (1999), arXiv:hep-ph/9906551.
 - [63] J. Wess and B. Zumino, Phys. Lett. **B37**, 95 (1971).
 - [64] E. Witten, Nucl. Phys. **B223**, 433 (1983).
 - [65] T. Schafer, Nucl. Phys. **A728**, 251 (2003), arXiv:hep-ph/0307074.
 - [66] P. Amore, M. C. Birse, J. A. McGovern, and N. R. Walet, Phys. Rev. **D65**, 074005 (2002), arXiv:hep-ph/0110267.
 - [67] M. Buballa, Phys. Lett. **B609**, 57 (2005), arXiv:hep-ph/0410397.
 - [68] M. M. Forbes and J. Kundu, in progress.
 - [69] S. R. Coleman, J. Wess, and B. Zumino, Phys. Rev. **177**, 2239 (1969).
 - [70] J. Callan, Curtis G., S. R. Coleman, J. Wess, and B. Zumino, Phys. Rev. **177**, 2247 (1969).

APPENDIX A: FULL PARAMETRIZATION

In this appendix, we give the full parametrization used to analyze the K^0 condensed states. First, we must introduce a full set of diagonal chemical potentials. One approach would be to introduce the 9 individual quark chemical potentials, but certain linear combinations couple to relevant physics. We fix the overall density by fixing the baryon chemical potential μ_B . Then we must enforce gauge neutrality, so we introduce μ_e which couples to the electromagnetic field, and the diagonal colour chemical potentials μ_3 and μ_8 . The rest of the chemical potentials are chosen to be orthogonal to these. Here then are the diagonal elements of the diagonal chemical potentials expressed as tensor products of the flavour and colour structure :

$$\mu_B \times [1, 1, 1] \otimes [1, 1, 1]/3, \quad (\text{A1a})$$

$$\mu_e \times [2, -1, -1] \otimes [1, 1, 1]/3, \quad (\text{A1b})$$

$$\mu_3 \times [1, 1, 1] \otimes [1, -1, 0]/2, \quad (\text{A1c})$$

$$\mu_8 \times [1, 1, 1] \otimes [1, 1, -2]/3, \quad (\text{A1d})$$

$$\mu_f \times [0, 1, -1] \otimes [1, 1, 1], \quad (\text{A1e})$$

$$\mu_{e3} \times [2, -1, -1] \otimes [1, -1, 0], \quad (\text{A1f})$$

$$\mu_{e8} \times [2, -1, -1] \otimes [1, 1, -2], \quad (\text{A1g})$$

$$\mu_{f3} \times [0, 1, -1] \otimes [1, -1, 0], \quad (\text{A1h})$$

$$\mu_{f8} \times [0, 1, -1] \otimes [1, 1, -2]. \quad (\text{A1i})$$

An alternative set of chemical potentials includes the hypercharge chemical potential μ_Y instead of μ_f . These are no longer orthogonal, but are still linearly independent.

$$\mu_B \times [1, 1, 1] \otimes [1, 1, 1]/3, \quad (\text{A2a})$$

$$\mu_e \times [2, -1, -1] \otimes [1, 1, 1]/3, \quad (\text{A2b})$$

$$\mu_3 \times [1, 1, 1] \otimes [1, -1, 0]/2, \quad (\text{A2c})$$

$$\mu_8 \times [1, 1, 1] \otimes [1, 1, -2]/3, \quad (\text{A2d})$$

$$\mu_Y \times [1, 1, -2] \otimes [1, 1, 1]/3, \quad (\text{A2e})$$

$$\mu_{e3} \times [2, -1, -1] \otimes [1, -1, 0], \quad (\text{A2f})$$

$$\mu_{e8} \times [2, -1, -1] \otimes [1, 1, -2], \quad (\text{A2g})$$

$$\mu_{f3} \times [0, 1, -1] \otimes [1, -1, 0], \quad (\text{A2h})$$

$$\mu_{f8} \times [0, 1, -1] \otimes [1, 1, -2]. \quad (\text{A2i})$$

The diagonal mass corrections (chiral condensates) do not couple to any external physics, so we simply use the nine quark mass corrections (δm_{ur} , δm_{ug} , δm_{ub} , δm_{dr} , δm_{dg} , δm_{db} , δm_{sr} , δm_{sg} , δm_{sb}).

The rest of the parameters are described in the following matrices. These appear more condensed when expressed in the basis described in [40] where the quarks are ordered (ru, gd, bs, rd, gu, rs, bu, gs, bd). In this basis, the matrices corresponding to the variational parameters

$$\mathbf{A} = \mathbf{1} \otimes \delta\mu + \gamma_5 \otimes \delta\mu_5 - \gamma_0 \otimes \delta\mathbf{m} - \gamma_0\gamma_5 \otimes \delta\mathbf{m}_5,$$

$$\mathbf{B} = \gamma_C\gamma_5 \otimes \Delta + \gamma_C \otimes \Delta_5 + \gamma_0\gamma_C\gamma_5 \otimes \kappa + \gamma_0\gamma_C \otimes \kappa_5.$$

In order to allow for a computer to enumerate the parameters, we introduce a systematic method for labelling the parameters. First, we use one of the names μ , μ^5 , m , m^5 , Δ , Δ^5 , κ , or κ^5 corresponding to the structure given above. We then use a two-digit index to specify which elements are non-zero and an i indicates that the specified element is i rather than simply 1. The symmetric entry must also be set so that the resulting matrix $\gamma \otimes \mu$ is either Hermitian or anti-symmetric depending on whether or not it parametrizes **A** or **B** respectively. In total, there are 666 independent matrices. For example

$$\mu_{12} = \mu_{12}^5 = \mathbf{m}_{12} = \Delta_{12} = \Delta_{12}^5 = \kappa_{12} = \begin{pmatrix} 0 & 1 & 0 & \cdots \\ 1 & 0 & 0 & \\ 0 & 0 & 0 & \\ \vdots & & & \ddots \end{pmatrix},$$

$$\mathbf{m}_{12}^5 = \kappa_{12}^5 = \begin{pmatrix} 0 & 1 & 0 & \cdots \\ -1 & 0 & 0 & \\ 0 & 0 & 0 & \\ \vdots & & & \ddots \end{pmatrix},$$

$$\mu_{12i} = \mu_{12i}^5 = \mathbf{m}_{12i} = \kappa_{12i}^5 = \begin{pmatrix} 0 & i & 0 & \cdots \\ -i & 0 & 0 & \\ 0 & 0 & 0 & \\ \vdots & & & \ddots \end{pmatrix},$$

$$\mathbf{m}_{12i}^5 = \Delta_{12i} = \Delta_{12i}^5 = \kappa_{12i} = \begin{pmatrix} 0 & i & 0 & \cdots \\ i & 0 & 0 & \\ 0 & 0 & 0 & \\ \vdots & & & \ddots \end{pmatrix}.$$

The reason that \mathbf{m}^5 and κ^5 behave differently than the others is that, while $\mathbf{1}$, γ_5 , and γ_0 are Hermitian, $\gamma_0\gamma_5$ is anti-Hermitian. Likewise, while $\gamma_C\gamma_5$, γ_C , and $\gamma_0\gamma_C\gamma_5$ are anti-symmetric, $\gamma_0\gamma_C$ is symmetric. Again, recall that these are all specified in the “unlocking” basis which is ordered as

$$\text{ru, gd, bs, rd, gu, rs, bu, gs, bd.} \quad (\text{A5})$$

The parity even CFL state with no mass or hypercharge is expressed in terms of this parametrization as

$$\Delta_{12} = \Delta_{13} = \Delta_{23} = (\Delta_3 + \Delta_6)/2, \quad (\text{A6a})$$

$$\Delta_{45} = \Delta_{67} = \Delta_{89} = (\Delta_6 - \Delta_3)/2, \quad (\text{A6b})$$

$$\Delta_{11} = \Delta_{22} = \Delta_{33} = \Delta_6, \quad (\text{A6c})$$

$$\mu_{12} = \mu_{13} = \mu_{23} = -3\mu_{\text{oct}}, \quad (\text{A6d})$$

$$\mu_{e3} = 3\mu_{e8} = -\mu_{f3} = \mu_{f8} = -3\mu_{\text{oct}}/4. \quad (\text{A6e})$$

Here are some comparisons with other conventions in the literature. Alford, Kouvaris, and Rajagopal [37] introduce Δ_1 , Δ_2 and Δ_3 which are all related to the attractive anti-symmetric $\bar{3}$ channel:

$$\Delta_{23} = \Delta_{89} = \Delta_1, \quad (\text{A7a})$$

$$\Delta_{13} = \Delta_{67} = \Delta_2, \quad (\text{A7b})$$

$$\Delta_{12} = \Delta_{45} = \Delta_3. \quad (\text{A7c})$$

Rüster, Shovkovy, and Rischke [39] introduces the parameters ϕ , φ and σ which include the repulsive symmetric 6 channel parameters:

$$\Delta_{23} = \varphi_1, \quad \Delta_{13} = \varphi_2, \quad \Delta_{12} = \varphi_3, \quad (\text{A8a})$$

$$\Delta_{89} = \phi_1, \quad \Delta_{67} = \phi_2, \quad \Delta_{45} = \phi_3, \quad (\text{A8b})$$

$$\Delta_{11} = \sigma_1, \quad \Delta_{22} = \sigma_2, \quad \Delta_{33} = \sigma_3. \quad (\text{A8c})$$

Finally, Buballa [67] uses only the following parameters to parametrize the meson condensed phases:

$$-\Delta_{12} = \Delta_{45} = s_{22}/4, \quad (\text{A9a})$$

$$-\Delta_{13} = \Delta_{67} = s_{55}/4, \quad (\text{A9b})$$

$$-\Delta_{23} = \Delta_{89} = s_{77}/4, \quad (\text{A9c})$$

$$-\Delta_{19i}^5 = \Delta_{47i}^5 = p_{25}/4, \quad (\text{A9d})$$

$$-\Delta_{18i}^5 = \Delta_{56i}^5 = p_{52}/4. \quad (\text{A9e})$$

In Tables II, III, IV, and V we give the numerical values of the parameters for each of the states displayed in Figures 1, 2, 5, and 6 respectively. We only list the non-zero parameters: the other parameters are zero.

Param.	$\mu_Y = 0.50\mu_Y^c$		$\mu_Y = \mu_Y^c$	
	Bare	Correction	Bare	Correction
$\mu_B/3$	+549.93	-49.93	+549.93	-49.93
μ_8	-12.5	+0	-25	+0
μ_Y	+12.5	+0	+25	+0
μ_{oct}	0	-0.031332	0	-0.031332
Δ_3	0	+25.657	+	+25.657
Δ_6	0	+0.65709	0	+0.65709

TABLE II: Parameters required for a self-consistent parity-even CFL solution in the presence of a hypercharge chemical potential. These values correspond to the dispersions shown in Figure 1. All values are in MeV. The first column labelled “Bare” gives the fixed bare parameters that enter the Hamiltonian (7). The column labelled “Correction” is the contribution from the self-energy. The sum of the columns is the value that enters the quadratic Hamiltonian (11).

Param.	$\mu_Y = 0.50\mu_Y^c$		$\mu_Y = 1.20\mu_Y^c$	
	Bare	Correction	Bare	Correction
$\mu_B/3$	+549.93	-49.932	+549.93	-49.947
μ_Y	+12.5	-1.0687	+30	-2.5931
μ_e	0	+0.53436	0	+1.2965
μ_3	-6.4772	-0.00000	-16.346	-3.331×10^{-7}
μ_8	-3.2386	-0.00000	-8.1729	-1.665×10^{-7}
μ_{e3}	0	+0.02421	0	+0.027856
μ_{e8}	0	+0.0080699	0	+0.0092853
μ_{f3}	0	+0.035998	0	+0.084801
μ_{f8}	0	+0.011999	0	+0.028267
$\mu_{12} = \mu_{18i}^5$	0	+0.016852	0	-0.047357
$\mu_{13} = \mu_{19i}^5$	0	+0.11902	0	+0.19694
$\mu_{23} = \mu_{89}$	0	+0.046967	0	+0.046617
μ_{28i}^5	0	+0.088616	0	+0.14526
$\mu_{29i}^5 = \mu_{38i}^5$	0	+0.046967	0	+0.046617
μ_{39i}^5	0	+0.0030234	0	-0.065811
μ_{46i}^5	0	+0.11479	0	+0.27514
Δ_{11}	0	+0.64468	0	+0.5851
$\Delta_{22} = -\Delta_{88} = -\Delta_{28i}^5$	0	+0.32265	0	+0.31566
$\Delta_{33} = -\Delta_{99} = -\Delta_{39i}^5$	0	+0.33523	0	+0.34523
$\Delta_{12} = -\Delta_{18i}^5$	0	+9.6383	0	+10.138
$\Delta_{13} = -\Delta_{19i}^5$	0	+8.9893	0	+8.5746
$\Delta_{23} = -\Delta_{89}$	0	+12.789	0	+12.605
$\Delta_{45} = -\Delta_{56i}^5$	0	-9.1811	0	-9.7012
$\Delta_{67} = -\Delta_{47i}^5$	0	-8.5229	0	-8.1128
$\Delta_{29i}^5 = \Delta_{38i}^5$	0	-0.33242	0	-0.35025

TABLE III: Parameters required for a self-consistent CFLK0 solution in the presence of a hypercharge chemical potential. These values correspond to the dispersions shown in Figure 2. All values are in MeV. The first column labelled “Bare” gives the fixed bare parameters that enter the Hamiltonian (7). The column labelled “Correction” is the contribution from the self-energy. The sum of the columns is the value that enters the quadratic Hamiltonian (11).

Param.	$M_s^2/(2\mu) = 0.50\mu_Y^c$		$M_s^2/(2\mu) = 0.83\mu_Y^c$	
	Bare	Correction	Bare	Correction
$\mu_B/3$	+549.93	-48.952	+549.93	-48.316
μ_8	-12.649	-0.00000	-20.95	$+1.469 \times 10^{-7}$
μ_{e3}	0	+0.022617	0	+0.022026
μ_{e8}	0	+0.0074542	0	+0.0072087
μ_{f3}	0	-0.022617	0	-0.022026
μ_{f8}	0	+0.022362	0	+0.021626
μ_{12}	0	+0.090467	0	+0.088103
$\mu_{13} = \mu_{23}$	0	+0.088963	0	+0.085669
$m_{ur} = m_{dg}$	0	+0.15778	0	+0.19366
$m_{ug} = m_{dr}$	0	+0.17255	0	+0.2117
$m_{ub} = m_{db}$	0	+0.15604	0	+0.19155
$m_{sr} = m_{sg}$	+61.843	+50.029	+80	+64.267
m_{sb}	+61.843	+50.079	+80	+64.329
m_{12}	0	-0.014765	0	-0.018037
$m_{13} = m_{23}$	0	+0.026496	0	+0.032723
$\Delta_{11} = \Delta_{22}$	0	-0.62077	0	-0.59745
Δ_{33}	0	-0.64043	0	-0.62926
Δ_{12}	0	-12.914	0	-12.753
$\Delta_{13} = \Delta_{23}$	0	-12.639	0	-12.302
Δ_{45}	0	+12.293	0	+12.155
$\Delta_{67} = \Delta_{89}$	0	+12.011	0	+11.693
κ_{11}	0	$+3.8762 \times 10^{-6}$	0	$+5.1011 \times 10^{-6}$
κ_{22}	0	$+3.8762 \times 10^{-6}$	0	$+5.0102 \times 10^{-6}$
κ_{33}	0	+0.078913	0	+0.098773
κ_{12}	0	+0.0017234	0	+0.0020923
$\kappa_{13} = \kappa_{23}$	0	+0.52751	0	+0.66061
κ_{45}	0	-0.0017195	0	-0.0020872
$\kappa_{67} = \kappa_{89}$	0	-0.48835	0	-0.61184

TABLE IV: Parameters required for a self-consistent parity even CFL solution in the presence of a strange quark mass. These values correspond to the dispersions shown in Figure 5. All values are in MeV. The first column labelled “Bare” gives the fixed bare parameters that enter the Hamiltonian (7). The column labelled “Correction” is the contribution from the self-energy. The sum of the columns is the value that enters the quadratic Hamiltonian (11). For example, the right set of data (just slightly before the CFL/gCFL transition) has a bare (current) strange quark mass of 80 MeV. This corresponds to a constituent quark mass of $80 + 64 \approx 144$ MeV. (Note that there is a slight difference for the blue constituent quark masses because of the presence of the coloured chemical potential μ_8 required to enforce neutrality.)

Param.	$M_s^2/(2\mu) = 0.50\mu_Y^c$		$M_s^2/(2\mu) = 0.84\mu_Y^c$	
	Bare	Correction	Bare	Correction
$\mu_B/3$	+549.93	-48.951	+549.93	-48.09
μ_3	-6.6057	-0.00000	-13.002	-8.7×10^{-8}
μ_8	-3.3029	-0.00000	-6.5008	-4.35×10^{-8}
μ_f	0	-0.53978	0	-1.0238
μ_{e3}	0	+0.023555	0	+0.025582
μ_{e8}	0	+0.0078516	0	+0.0085274
μ_{f3}	0	+0.035852	0	+0.066184
μ_{f8}	0	+0.011951	0	+0.022061
$\mu_{12} = \mu_{18i}^5$	0	+0.014623	0	-0.026924
$\mu_{13} = \mu_{19i}^5$	0	+0.11615	0	+0.16265
$\mu_{23} = \mu_{89}$	0	+0.044694	0	+0.042908
μ_{28i}^5	0	+0.086431	0	+0.11903
$\mu_{29i}^5 = \mu_{38i}^5$	0	+0.044644	0	+0.042927
μ_{39i}^5	0	-0.001146	0	-0.047235
μ_{46i}^5	0	+0.11528	0	+0.21622
$m_{ug} = -m_{ub}$	0	+0.0077476	0	+0.0093125
m_{dr}	0	+0.17093	0	+0.21503
$m_{dg} = m_{db}$	0	+0.15529	0	+0.19536
m_{sr}	+61.637	+50.279	+85	+69.188
$m_{sg} = m_{sb}$	+61.637	+50.335	+85	+69.301
$m_{12} = -m_{18i}^5$	0	-0.010709	0	-0.013162
$m_{13} = -m_{19i}^5$	0	+0.029548	0	+0.053931
$m_{23} = m_{89}$	0	+0.0134	0	+0.017695
$m_{29i}^5 = -m_{38i}^5$	0	-0.012525	0	-0.01659
m_{46i}^5	0	-0.0077707	0	-0.009337
Δ_{11}	0	+0.60701	0	+0.53896
$\Delta_{22} = -\Delta_{88}$	0	+0.30409	0	+0.28263
$\Delta_{33} = -\Delta_{99}$	0	+0.32668	0	+0.32494
$\Delta_{12} = -\Delta_{18i}^5$	0	+9.4718	0	+9.6392
$\Delta_{13} = -\Delta_{19i}^5$	0	+8.614	0	+8.0104
$\Delta_{23} = -\Delta_{89}$	0	+12.282	0	+11.726
$\Delta_{45} = -\Delta_{56i}^5$	0	-9.0411	0	-9.2445
$\Delta_{67} = -\Delta_{47i}^5$	0	-8.1684	0	-7.5847
Δ_{28i}^5	0	-0.30382	0	-0.28208
$\Delta_{29i}^5 = \Delta_{38i}^5$	0	-0.31799	0	-0.31604
Δ_{39i}^5	0	-0.32038	0	-0.31321
$\kappa_{22} = -\kappa_{88}$	0	-1.7029×10^{-5}	0	-1.3167×10^{-5}
$\kappa_{33} = -\kappa_{99}$	0	-0.040639	0	-0.055178
$\kappa_{12} = \kappa_{18i}^5$	0	-0.00066095	0	-0.00090186
$\kappa_{13} = \kappa_{19i}^5$	0	-0.36095	0	-0.46324
$\kappa_{23} = -\kappa_{89}$	0	-0.50626	0	-0.66374
$\kappa_{45} = -\kappa_{56i}^5$	0	+0.00075037	0	+0.001152
$\kappa_{67} = \kappa_{47i}^5$	0	+0.33313	0	+0.4268
$\kappa_{29i}^5 = -\kappa_{38i}^5$	0	-0.019786	0	-0.026852

TABLE V: Parameters required for a self-consistent CFLK0 solution in the presence of a strange quark mass. These values correspond to the dispersions shown in Figure 6. All values are in MeV.